Acta Biomaterialia xxx (xxxx) xxx

Contents lists available at ScienceDirect

Acta Biomaterialia

journal homepage: www.elsevier.com/locate/actbio

Full length article

Generation of 3D melanoma models using an assembloid-based approach

Daniel B. Rodrigues[a,b], Helena R. Moreira[a,b], Mariana Jarnalo[c,d], Ricardo Horta[c,d], Alexandra P. Marques[a,b], Rui L. Reis[a,b], Rogério P. Pirraco[a,b,*]

[a] 3B's Research Group, I3Bs – Research Institute on Biomaterials, Biodegradables and Biomimetics, University of Minho, Headquarters of the European Institute of Excellence on Tissue Engineering and Regenerative Medicine, AvePark, Parque de Ciência e Tecnologia, Zona Industrial da Gandra, 4805-017 Barco, Guimarães, Portugal
[b] ICVS/3B's – PT Government Associate Laboratory, Braga, Guimarães 4805-017, Portugal
[c] Department of Plastic and Reconstructive Surgery, and Burn Unity, Centro Hospitalar de São João, Porto, Portugal
[d] Faculty of Medicine - University of Porto, Portugal

ARTICLE INFO

Article history:
Received 25 July 2023
Revised 31 January 2024
Accepted 13 February 2024
Available online xxx

Keywords:
Assembloids
Tumor models
Melanoma
Spheroids
3D models

ABSTRACT

While 3D tumor models have greatly evolved over the past years, there is still a strong requirement for more biosimilar models which are capable of recapitulating cellular crosstalk within the tumor microenvironment while equally displaying representative levels of tumor aggressiveness and invasion. Herein, we disclose an assembloid melanoma model based on the fusion of individual stromal multicellular spheroids (MCSs). In contrast to more traditional tumor models, we show that it is possible to develop self-organizing, heterotypic melanoma models where tumor cells present stem-cell like features like up-regulated pluripotency master regulators SOX2, POU5F1 and NANOG. Additionally, these assembloids display high levels of invasiveness while embedded in 3D matrices as evidenced by stromal cell promotion of melanoma cell invasion via metalloproteinase production. Furthermore, sensitivity to anticancer drug doxorubicin was demonstrated for the melanoma assembloid model. These findings suggest that melanoma assembloids may play a significant role in the field of 3D cancer models as they more closely mimic the tumor microenvironment when compared to more traditional MCSs, opening the doors to a better understanding of the role of tumor microenvironment in supporting tumor progression.

Statement of significance

The development of complex 3D tumor models that better recapitulate the tumor microenvironment is crucial for both an improved comprehension of intercellular crosstalk and for more efficient drug screening. We have herein developed a self-organizing heterotypic assembloid-based melanoma model capable of closely mimicking the tumor microenvironment. Key features recapitulated were the preservation of cancer cell stemness, sensitivity to anti-cancer agents and tumor cell invasion promoted by stromal cells. The approach of pre-establishing distinct stromal domains for subsequent combination into more complex tumor constructs provides a route for developing superior tumor models with a higher degree of similarity to native cancer tissues.

© 2024 The Author(s). Published by Elsevier Ltd on behalf of Acta Materialia Inc.
This is an open access article under the CC BY license (http://creativecommons.org/licenses/by/4.0/)

1. Introduction

Skin melanoma is a malignant neoplasm that arises from the uncontrolled proliferation of melanocytes. While only accounting for about 1 % of all skin cancer cases, it is responsible for the vast majority of skin cancer deaths making it the most aggressive form of this cancer [1]. In 2022, in the US alone, 99,780 new cases of melanoma are expected to be diagnosed followed by 7650 deaths [2].

Three-dimensional (3D) tumor models such as multicellular spheroids (MCSs), organoids and organotypic melanoma skin models [3–5] are increasingly considered as key tools in the path towards the development of more effective cancer therapies [6]. MCS, in particular, became popular in the field [7–10] due to the

* Corresponding author.
E-mail address: rpirraco@i3bs.uminho.pt (R.P. Pirraco).

https://doi.org/10.1016/j.actbio.2024.02.023
1742-7061/© 2024 The Author(s). Published by Elsevier Ltd on behalf of Acta Materialia Inc. This is an open access article under the CC BY license (http://creativecommons.org/licenses/by/4.0/)

Please cite this article as: D.B. Rodrigues, H.R. Moreira, M. Jarnalo et al., Generation of 3D melanoma models using an assembloid-based approach, Acta Biomaterialia, https://doi.org/10.1016/j.actbio.2024.02.023

ease in obtaining heterotypic 3D systems that share similar traits to the native tumor and tumor microenvironment. MCSs consist in cell aggregates that exhibit complex cell-cell and cell-matrix interactions, resulting in the formation of a gradient for nutrients, gases, growth factors and signaling factors. Morphologically, they present a variable 3D architecture which is highly dependent on factors such as cell type, cell density, culture method and mechanical stress [11].

Despite this availability of 3D tumor models, several issues still remain. One must consider that melanoma progression is driven by the reciprocal interactions among the different cell types that make up the tumor microenvironment in addition to malignant cells themselves [12–14]. This accounts for paracrine interactions orchestrated among fibroblasts, endothelial cells, immune cell and other neighboring cells that contribute to the complexity and heterogeneity of this cancer, complicating the precise recapitulation of tumor features within the current models. These have critical limitations such as the lack of a vascular compartment and immune cells, the inability to perfectly recreate tissue-tissue interfaces as well as to control the spatiotemporal distribution of nutrients and waste, ultimately rendering these models unable to mimic the development factors that regulate cell growth and differentiation in vivo [15]. Some authors have attempted to overcome some of these issues by partitioning the formation of these 3D systems over time [16,17], by adding specific cells or molecular cues at specific timepoints but with limited success. Therefore, the need for state-of-the-art complex models capable of thoroughly mimicking cell interactions to better understand tumor development and progression and to facilitate drug development, is clear.

Assembloids are considered a step forward in the development of tissue specific organoids. They were first created with the intent of combining multiple brain regions and/or cell lineages in 3D culture to model interactions among them and allow the study of cell-cell interactions as well as the assembly of neural circuits. This conceptualization came to life through the development of separate organoids resembling dorsal and ventral forebrain and then fusing them together into a multi-region assembloid [18–21]. Several advantages of this system have been identified, namely the underlying possibility of maturing and tailoring individual organoids before fusion and replicating region-specific interfaces within tissues, and also the longer viability time due to the more native-like representation of living systems [21,22].

Here, we developed different melanoma stromal compartments by using MCSs comprising co-cultures of a human melanoma cell line (VMM15), human dermal endothelial cells (hDMECs), human adipose derived stem cells (hASCs) and human dermal fibroblasts (hDFbs) which were then fused into a melanoma-like assembloid. We dissected the impact of stromal crosstalk in melanoma 3D invasion and the active role of metalloproteinases (MMPs). Most importantly, we established a 3D model that better recapitulates the complexity and heterogeneity of human skin melanoma.

2. Materials and methods

2.1. Cell lines and culture conditions

hTERT Dermal Microvascular Endothelial Cell, Neonatal (ATCC® CRL-4060™) were obtained from ATCC and were cultured in Vascular Cell Basal medium (ATCC, USA) supplemented with the Microvascular Endothelial Cell Growth Kit – BBE (ATCC. USA) or EGM-2 MV Microvascular Endothelial Cell Growth Medium-2 BulletKit (Lonza, USA). Human dermal fibroblasts (hDFbs) and human adipose derived stem cells (hASCs) were harvested from human skin samples obtained from abdominoplasties after written informed consent and under the protocol Nr 477/2020 approved by the Ethical Committee of Hospital S. João (Porto, Portugal). Both hDFbs and hASCs were cultured in α-MEM, supplemented with 10% fetal bovine serum (FBS, Invitrogen, USA) and human cell line VMM15 (ATCC® CRL-3227™), derived from metastatic melanoma lesions, were grown as adherent cultures in RPMI 1640 supplemented with 10% fetal bovine serum (FBS), l-glutamine (2 mmol/L), penicillin (100 units/mL), and 1% antibiotic/antimycotic. All cells were kept in culture at 37 °C in a humidified atmosphere under 5% CO2.

2.2. Generation and analysis of tumor spheroids

To produce the intended spheroids, several different cell combinations were performed to mimic independent tumor cell niches. Cell ratios and culture conditions were optimized to achieve optimal spheroid formation and growth. Co-cultures of tumor cells and hDFbs were achieved by mixing 5000 tumor cells with 15,000 hDFbs which were then seeded into wells of ultra-low attachment (ULA) 96-well round-bottomed plates (Corning, Amsterdam, The Netherlands) and were thereafter cultured in standard culture conditions. Co-culture spheroids of hDMECs were achieved by culturing 10,000 endothelial cells with 30,000 cells of either hDFbs or hASCs. For assembloid formation, individual spheroids were allowed to stabilize for 3 days before being placed in combinatorial culture for an additional 10 days. Individual co-culture spheroids and assembloids formed without the tumor cell compartment were used as controls. Additionally, multicellular control spheroids comprising all of the cellular constituents in the same densities as used in the tumor assembloids were also established. In this condition a mixture of 5000 tumor cells, with 45,000 hDFbs, 20,000 endothelial cells and 30,000 hASCs were added all at once at day 0 and cultured for a total of 13 days.

2.3. ICC and IHC

2.3.1. Co-culture immunocytochemistry/immunohistochemistry

At each relevant time-point, spheroids were fixed in methanol for 15 min and were transferred into Tissue-Tek Cryomolds (Sakura Finetek, Netherlands) wells containing HistoGel™ (Thermo Scientific, Ireland) for subsequent paraffin embedding. Samples were then sectioned to obtain 4-μm slices. Tissue sections were stained with Haematoxylin & Eosin (Sigma, USA) and Picrosirius Red kit (Bio-Optica, Italy) following routine protocols. For immunohistochemistry, paraffin tissue sections were deparaffinized in xylene, re-hydrated and boiled for 5 min in Tris-EDTA buffer (10 mM Tris Base, 1 mM EDTA solution and, 0.05% (v/v) Tween 20, pH 9) for antigen retrieval. Afterwards, sections were permeabilized with 0.2% Triton X-100 and unspecific staining was blocked with 3% Bovine Serum Albumin (Sigma). For primary antibodies, we used mouse monoclonal antibody to CD-31 (Dako, Denmark) at 1:30, rabbit polyclonal antibody to GP100 (Abcam, UK) at 1:300 or rabbit monoclonal antibody to Ki-67 at 1:50 (Abcam, UK) which were incubated overnight at 4 °C. For detection, secondary antibodies were incubated at RT for 1 h at 1:500 dilution. Nuclei were counter-stained with DAPI. Histological staining's were examined under a Leica DM750 microscope, using LEICA Application Suite 4.13.0 while immunofluorescence labelling was acquired under a Zeiss Axio Imager Z1m with ZEN 3.2 software (blue edition).

2.3.2. Whole spheroid immunohistochemistry

To evaluate the cellular participation in the formation of capillary like structures and cell invasion, individual co-cultured spheroids or assembloids where transferred to ultra-low attachment (ULA) 96-well round-bottomed plates (Corning, Amsterdam, The Netherlands) at each respective time-point and were fixed in methanol for 15 min after which they were left to clear in Scale-A2 for 7 d After this period samples were re-hydrated for 10 min in PBS. Whole spheroids were then permeabilized/blocked for 2 h in

0.1% Triton X-100 (wt/vol)/10 % fetal bovine serum (vol/vol)/PBS (B-PBT) and then processed by free-floating immunohistochemistry. For double staining, primary antibodies from different species were incubated simultaneously, followed by incubation with secondary antibodies. For primary antibodies, we used mouse monoclonal antibody to CD-31 (Dako, Denmark) at 1:30 and rabbit polyclonal antibody to GP100 (Abcam, UK) at 1:300 diluted in B-PBT with 4′,6-diamidino-2-phenylindole (DAPI) at a 1:1000 dilution overnight. Spheroids underwent two 2 h washes with 0.2 % Triton X-100 in PBS (PBT), followed by one 2 h B-PBT wash and subsequently were incubated with secondary antibodies at 1:200 in B-PBT with DAPI at a 1:1000 dilution overnight. Spheroids underwent two 2 h PBT washes and returned to the clearing solution. Whole spheroid imaging was performed under a Leica TCS SP8 with Leica Application Suite X 3.5.7.

2.3.3. Immunocytochemistry evaluation of invasive migratory behavior

To study the cellular migratory behavior of the developed assembloids and MCSs throughout a 3D basement membrane-like matrix, Matrigel®-embedded spheroids were fixed after 7 days in 4% paraformaldehyde (vol/vol) (Thermo Scientific, Ireland) in PBS for 90 min at 37 ºC. A 0.5% Triton X-100 (wt/vol) permeabilization solution was prepared in PBS, added to the embedded spheroids and left overnight to incubate at 4 °C. The following day, the spheroids were blocked in 5 % FBS (vol/vol) in PBS for 2 h at room temperature followed by a 4 h incubation with rabbit polyclonal antibody to GP100 (Abcam, UK) at 1:50 diluted in PBS. Unbound primary antibody was washed away with PBS through three repetitive washes at room temperature. Subsequently, spheroids were incubated overnight at 4 ºC with secondary antibody at 1:200 in PBS. To this secondary antibody solution was also added DAPI (1:1000 dilution) and phalloidin-TRITC (1:25 dilution). After washing three times with PBS, the embedded spheroids were ready for visualization. Imaging was performed using a Zeiss LSM 980 AiryScan 2 confocal microscope working with ZEN 3.6 software (blue edition).

2.3.4. Sample clearing

In order to achieve refractive index matching of the developed spheroids and assembloids for microscopy acquisition, the aqueous-based clearing solution ScaleA2 [23] was prepared by mixing stock solutions for a final concentration of 4 m urea (Sigma, USA), 0,1 % Triton X-100 (Sigma, USA) and 10 % glycerol (Honeywell, Germany) according to [23].The volume was adjusted by diluting the mixed solutions with water.

2.4. Real-time PCR gene expression analysis

Total RNA was extracted from cells using RNeasy Mini Kit (Qiagen, Germany) and quantified using a spectrophotometer NanoDrop N-1000 (Thermo Fischer Scientific, USA). 250 ng of RNA was retrotranscribed in cDNA with the QSCript cDNA SuperMix (Quanta Biosciences, USA). The qPCR reactions were all per-formed in triplicate. The predesigned Taqman primers (Thermo Fisher, USA) were: *SOX2* Hs01053049_s1; *POU5F1* Hs00999632_g1; *NANOG* Hs04399610_g1; *SIRT1* Hs01009006_m1; *TINF2* Hs00173291_m1; *TERF2* Hs00194619_m1; *B2M* Hs00187842_m. Data from these Taqman primers was normalized to hDMECs/hASCs MCSs due to the known expression for these markers in hASCs. Forward and reverse human specific primers used are as follows: *TP53BP1* 5′-AAATCCTTCAGCCGTGTCGT-3, 5′-AGTCACTACGACGCAAAGCA-3; *BRCA1* 5′-GTCCCATCTGTCTGGAGTTGA-3, 5′-GGCCCTTTCTTCTGGTTGAGA-3; *B2M* 5′-TGGAGGCTATCCAGCGTACT-3, 5′-CGGATGGATGAAACCCAGACA-3; *CDH2* 5′-TCAGGCGTCTGTAGAGGCTT-3, 5′-ATGCACATCCTTCGATAAGACTG-3; *ZEB1* 5′-TAAGCGCAGAAAGCAGGCGAA −3, 5′-TCTGTAACACTTTCTTCTTCCACAATATGC-3; *CDH1* 5′-CAGTCAAAAGGCCTCTACGG-3, 5′-CCCACTGTATTCAGCGTGAC-3; *VIM* 5′-GCTTCAGAGAGAGGA-3, 5′-AAGGTCAAGACGTGCCAGAG-3. These genes were normalized to VMM15/hDFbs MCSs. The cycle-threshold was automatically calculated using QuantStudio™ Design & Analysis Software v1.5.2 (Applied Biosystems, Life Technologies, UK), and *B2M* was used as an endogenous control. The relative expression levels of mRNAs were calculated using the Livak method by the equation $2^{-\Delta\Delta Ct}$.

2.5. Labeling of spheroids with CellTracker™ dyes

Spheroids were individually labeled for live tracking. hDMECs/hDFbs were labelled with Cell Tracker™ Green CMFDA, hDMECs/hASCs with Cell Tracker™ Orange CMRA and VMM15/hDFbs with Cell Tracker™ Blue dye. For this effect a mixture of basal serum free EGM2-MV and 10 μM CellTracker™ solution in dimethyl sulfoxide (DMSO) (VWR, USA) was prepared. To the free-floating spheroid, standard growing medium was removed from the culture plate; cells were rinsed twice with phosphate buffer (PBS, Gibco, USA) and the prepared mixture was added. After 1 h incubation at 37 °C, the spheroids were washed and left in complete culture medium for time-lapse microscopy.

2.6. Assembloid response to chemotherapeutic treatment

To determine the cellular cytotoxicity of a known chemotherapeutic compound on both assembloids and MCSs, spheroids were treated with Dox overtime. For this effect, at 10 d of assembloid culture, medium was switched to a solution of 40 μM Dox diluted in culture medium for an additional 4 d culture period. Cells lysates and culture medium samples were recovered to determine LDH activity. CyQUANT LDH Cytotoxicity Assay Kit (Invitrogen™, USA) was used, according to manufactures instructions, to measure the levels of the cytosolic enzyme released into the cell culture medium upon damage to the plasma membrane. Absorbance at 490 nm and 680 nm were measured using a Multi-Detection Microplate Reader (SYNERGY HT, BIO-TEK, USA).

2.7. Metalloproteinase production by assembloids

Conditioned media was collected from the cultures at day 4, 7 and 10 after starting the combinatorial culture of the independently formed spheroids and stored at −80 °C (pooling of samples was performed). Protein concentration in the sample was measured using Bradford method, and 20 μg of protein was electrophoretically resolved for each sample in 10 % SDS-PAGE containing 0.1% gelatin (Sigma-Aldrich, USA) as the MMP substrate. Gels were washed twice for 30 min in renaturing buffer (2 % v/v Triton X-100) at room temperature to remove SDS, rinsed for 5 min in developing buffer (500 mM Tris–HCl, 2 M NaCl, 50 mM CaCl2), and then incubated for 24 h in developing buffer at 37 °C. The gel was stained with 0.1% R-250 Coomassie staining solution for 1 h at room temperature followed by destaining (50 % v/v methanol and 10 % v/v acetic acid in dH_2O) until MMP activity was detected in the gel as clear bands against a dark blue background. Band intensity was quantified using the Image Studio Ver. 5.2 software. Values were normalized to the control sample in each gel and expressed as relative densitometric units.

2.8. TIMP-1 and TIMP-2 production by assembloids

ELISA (Abcam, UK) was used to quantify the levels of both TIMP-1 and TIMP-2 released 10 days after starting the combinatorial culture of the independently formed spheroids. Conditioned media was collected from the cultures at day 10 and used to carry

out the procedure according to the manufacturer's instructions. 5 μg of total protein were used to carry out the quantification of TIMP-1 while 20 μg were used for TIMP-2. The absorbance was read at 600 nm in a kinetic manner for TIMP-1 and for TIMP-2 absorbance was read at 450 nm using a Synergy HT (BioTek, Vermont, USA) microplate reader. The quantity of both TIMP-1 and TIMP-2 protein were determined by means of a standard curve. Both proteins within the control media were undetectable during the experiments and therefore were omitted from the figures.

2.9. Tumor spheroid-based Matrigel invasion assay

For 10 d cultured assembloids, 50% of the culture medium volume was removed and replaced with an equal volume of stock Matrigel® (BD Biosciences, Oxford, UK). The culture plate was immediately centrifuged (300 g 3 min) at 4 ºC and stored for matrixgel solidification (1 hr 37 ºC). Over subsequent days (i.e. Day 0 to +7) spheroid growth and invasion was captured by bright-field microscopy (grey-scale images, Axio Observer microscope, AxioCam MR R3 camera 1388×1040 pixel resolution). Analysis settings were adjusted to achieve an optimal image segmentation that also reflects the degree of invasion.

2.10. Image analysis by Insidia macro

For post-processing image analyses of spheroid area and circularity, the FIJI [24] macro "Analyze Spheroid Cell Invasion In 3D Matrix, RRID:SCR_021204″ was used. To determine assembloid and spheroid invasion in Matrigel®, grey-scale images were organized into the required file structure for automatic batch processing. Spheroid segmentation and analysis was performed with the INSIDIA (INvasion SpheroID ImageJ Analysis) [25] macro for FIJI. Considering that spheroid core size has shown to lead to misinterpretations regarding net invasion, the area of invasive edge was normalized on the area of the core.

2.11. Statistical analysis

Data are expressed as mean ±standard deviation of three independent experiments. Shapiro–Wilk test was performed to validate normality of data prior to statistical testing. Statistical analysis was performed using one-way of two-way analysis of variance (ANOVA), followed by either a Tukey's or Bonferroni's multiple comparison post hoc test. Significance was set to 0.05 (95% of confidence interval). Significance levels were analyzed with GraphPad Prism statistical software v8.0 (GraphPad Software, USA) and indicated as p values ($^{*}p$ <0.05, $^{**}p$ <0.01, and $^{***}p$ <0.001).

3. Results

3.1. Differential 3D co-culture of endothelial cells impacts vascular network formation

To create a 3D model capable of mimicking the tumor microenvironment to a certain degree of resemblance one must understand the cellular nature of the tumor microenvironment in which cellular interplay is key. Endothelial cells have been shown to provide different cell responses dependent on different stimuli, be it from stromal fibroblasts [26], extracellular matrix [27] or stem cells [28]. Additionally, direct cell-cell contact between melanoma cells and stromal fibroblasts has been shown to drive functional interactions [29], while it has also been shown that adult mesenchymal stem cells impact tumor cell behaviour [30]. With this in consideration, we paired specific stromal cells found in the tumor microenvironment producing three distinct MCSs which were further fused to achieve an assembloid melanoma model. Each of these subdomains are representative of distinct cellular interactions that occur within a solid tumor i) an endothelial cell/fibroblast domain (hDMECs/hDFbs); ii) an endothelial/stem cell domain (hDMECs/hASCs) and iii) a tumoral/fibroblast (VMM15/hDFbs) domain. These spheroids were characterized in terms of area and circularity. A distinct architecture was seen for each of the developed MCSs (Fig. 1a*ii*), with the hDMECs/hDFbs spheroids comprising in average an approximate area of 2.4 × 10^5 μm^2, while the combination of hDMECs/hASCs yielded a significantly greater area of 3.86×10^5 μm^2. Finally, the co-culture of VMM15/hDFbs yielded an area of approximately 2.85×10^5 μm^2. Circularity data indicated a high circularity score of approximately 0.8 regardless of the spheroid system considered, where 1 would be indicative of perfect circularity.

The hematoxylin and eosin (H&E) staining (Fig. 1a*i*) of the produced 3D spheroids after a 3-day cultivation period revealed a compact structure regardless of the co-cultured cells. Both conditions where hDMECs were present displayed a preferential alignment with densely arranged clusters of cells towards the center. The tumor MCSs displayed characteristic tumor cell nuclei including nuclear enlargement and increased nuclear-to- cytoplasm ratio. Evidence of some karyorrhexis was found towards the core region of hDMECs co-cultured MCSs. Picrosirius red (PSR) was used to provide insights regarding collagen distribution within the produced MCSs (Fig. 1a*i*). When comparing the 3 developed MCSs, it was evident that the cross-talk between the used cells was creating distinct collagen deposition signatures. The co-culture of hDMECs/hDFbs revealed dense deposition of collagen fibers distributed throughout the whole spheroid. Interestingly, near the surface, these spheroids displayed an aligned deposition of fibers surrounding the core. The condition comprising hDMECs/hASCs, while having a similar cellular density than hDMECs/hDFbs, presented a distinct collagen signature, with it being distributed essentially towards the spheroid core. VMM15/hDFbs on the contrary, despite fibroblasts being typically strong collagen-producing cells, presented little collagen deposition in comparison with the other conditions.

Considering the differences in collagen deposition and cellular arrangement among the developed MCSs, we investigated if this would impact the 3D architecture and organization of the hDMECs within each spheroid. Whole-spheroid confocal imaging of CD31 immunolabeled samples showed a distinct reorganization of the hDMECs compartment among both conditions analyzed (Fig. 1b). hDMECs/hDFbs MCSs presented dense capillary-like networks at days 7 and 14 of culture, with hDMECs concentrating in the inner core at later timepoints. However, such capillary-like networks were not seen in hDMECs/hASCs MCSs, where clusters of hDMECs were distributed throughout the spheroid.

In sum, the MCSs demonstrated differential deposition of collagen rich extracellular matrix, as well as differential organization of hDMECS with formation of capillary-like structures only in the presence of hDFbs. With this in consideration, these different subdomains were assembled into a larger heterotypic system to understand their interplay and how they assist in tumor progression.

3.2. Obtaining complex assembloids based on combinatorial culture of MCSs building blocks

To carry out the development of the tumor assembloid system, we took into consideration the previous results and defined a 3-day priming period for each spheroid niche to self-organize without the influence of any additional cell type. After this period, the 3 MCSs were placed in combinatorial culture to interact over an additional 10-day period. Their fusion was analyzed over 7 days through time-lapse microscopy, after labelling each subset with a different colored cell tracker (Fig. 2a)**(Video S1, Supporting Infor-**

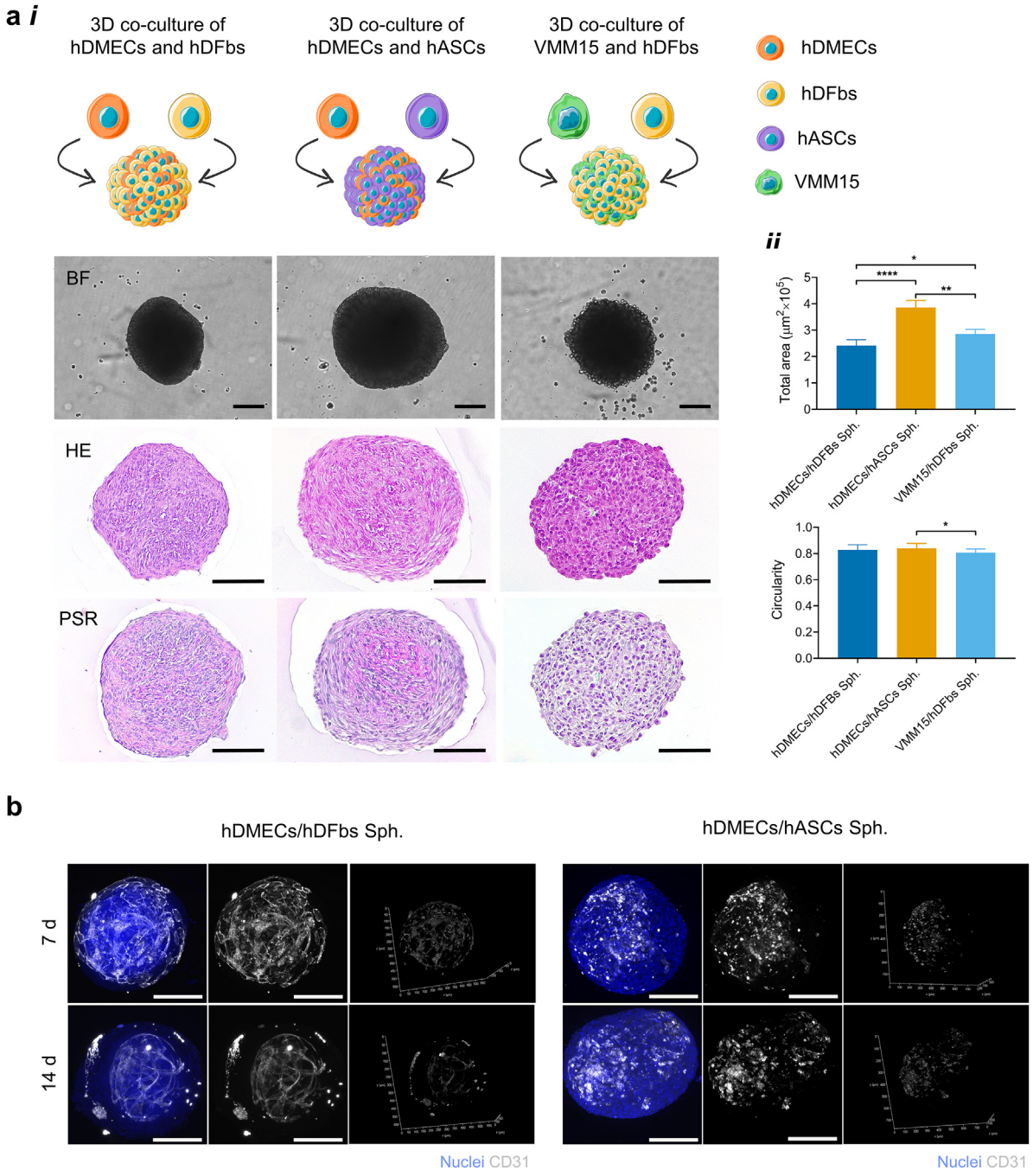


Fig. 1. Production of stromal MCS as building blocks for assembloid formation. ai) Schematic representation of the production of MCSs. Representative hematoxylin and eosin (H&E) and PSR staining of paraffin-embedded MCSs sections. Scale bar, 200 μm. aii) Characterization of total area and circularity score of the described MCSs. b) Representative immunocytochemistry images of the organization of CD31$^+$ endothelial cells in MCSs sections over 7 and 14 days (d) of culture. Nuclei were counterstained with DAPI. Scale bar = 100 µm. Quantitative results are expressed as the mean ± standard deviation where $n = 3$, * $p < 0.05$, ** $p < 0.01$, **** $p < 0.0001$, one-way ANOVA with Kruskal–Wallis multiple comparison post-test.

mation). Spheroid fusion was verified to begin as early as 24 h and was concluded around day 7 when the individual subdomains were no longer visible and a singular assembloid structure was obtained. Spheroid fusion appeared to occur in a specific order in which the hDMECs/hASCs fused around the hDMECs/hDFbs compartment and ultimately were surrounded by the VMM15/hDFbs MCS. To evaluate the cellular organization and histoarchitecture of the assembloid, HE and PSR stainings as well as immunolabelling were performed. Two different control conditions were prepared. The first consisted in hDMECs/hASCs spheroids placed in combinatorial culture with hDMECs/hDFbs spheroids (CTRL assembloid), lacking therefore the tumoral compartment of the tumor assembloid. The second control condition consisted in a multicellular spheroid (CTRL MCS) in which all cell types present in the individual spheroids used to obtain the tumor assembloid were added at the same time, at day 0. During culture, it was observed that cells in the CTRL MCS tended to form aggregates outside the main spheroid **(Figure S1, Supporting Information)**, driving an irregular distribution of cells over the outer spheroid layer (e. g. bulge formation) and increasing the heterogeneity of replicates, with likely consequences on the reliability of downstream assays.

After a total of 13 days of culture (3 days of pre-conditioning followed by 10 days of combinatorial culture), a clear layered structure was evidenced by HE staining (Fig. 2b) in both tumor and con-

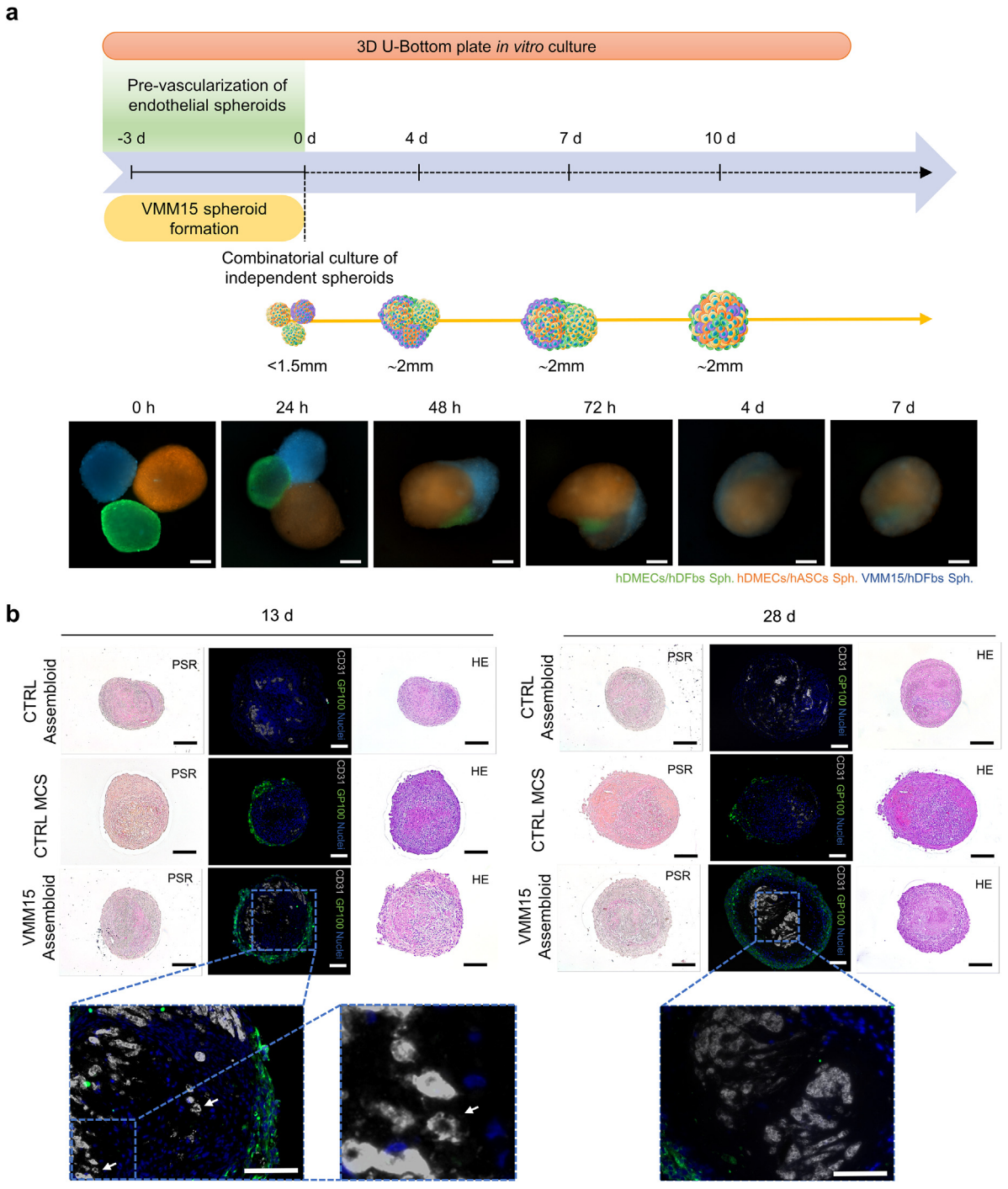


Fig. 2. Assembly of structured MCSs into complex melanoma models. a) Schematic representation of the process of production of the melanoma assembloid model. Time-lapse of MCSs fusion over 7 d hDMECs/hDFbs were labelled with Cell Tracker™ Green CMFDA, hDMECs/hASCs with Cell Tracker™ Orange CMRA and VMM15/hDFbs with Cell Tracker™ Blue dye. b) Representative H&E and PSR staining of paraffin-embedded MCSs sections. Scale bar, 200 μm. Representative immunocytochemistry images of the organization of CD31$^+$ and GP100$^+$ cells in the developed assembloids and CTRL MCS over 13 and 28 d of culture. Nuclei were counterstained with DAPI. Arrows depict structures resembling lumens. Scale bar = 100 µm. (For interpretation of the references to color in this figure legend, the reader is referred to the web version of this article.)

trol assembloids, with no visible necrosis. Cell clusters arranged towards the core were comprised of CD31$^+$ endothelial cells as seen by immunolabelling. Additionally, a vast deposition of collagen, stained in red by PSR, was visible in both conditions but denser in the regions where hDMECs were found to be present. In the melanoma assembloid system, an outer cell layer comprising enlarged nuclei and an increased nuclear-to- cytoplasmic ratio was visible, which overlapped with immunolabeling for the melanoma antigen GP100. These GP100 positive tumor cells distributed themselves in a manner in which they encapsulated the VMM15 assembloid, resembling an outer ring which measured approximately 39.29 $\pm$ 3.34 μm in thickness. When analyzing the distribution of the hDMECs within the melanoma assembloid, structures resembling lumens were found. In the CTRL MSC, an irregular distribution of tumor cells over the surface was observed by HE staining and confirmed by positive staining for GP100. Collagen staining, by PSR, showed decreased deposition of this protein when compared to both assembloid conditions. Cells positive for CD31 were few

in this condition and didn't show any organization. When extending the culture period to a total of 28 days (Fig. 2b), a very slight increase in collagen deposition was verified for this control condition while a significant loss of GP100-positive tumor cells throughout the surface was visible. For the assembloid conditions, a more extensive reorganization of the collagen fibers in circular patterns was present in both tumor and CTRL assembloids at 28 days. This patterned deposition of collagens was coincident with an organized cellular layering as seen by HE. Lack of nuclei staining at the core is highly suggestive of necrosis. Proliferative cells were then identified in the VMM15 assembloids using Ki-67 immunofluorescence staining procedure **(Figure S2, Supporting Information)**. We observed that, at 13 days of total culture time, these assembloids displayed a homogeneous Ki-67 positive cell distribution pattern along the outermost layers, where $GP100^{+}$ cells were previously shown to locate. After 28 days of total culture time, no Ki-67 positive cells were found.

Given that the VMM15 cell line is of metastatic origin, the expression of the known core pluripotency stem cell master regulators octamer-binding factor 4 (OCT4/POU5F1), SRY box-containing factor 2 (SOX2), and NANOG was then evaluated. While these factors have been associated to the regulation of self-renewal and pluripotency in adipose tissue adult stem cells [31,32], within tumors their expression has been associated to tumor transformation, tumorigenicity, tumor metastasis[33] as well as treatment resistance [34]. Firstly, the expression of these pluripotency regulators in 2D monocultures of each of the utilized cells types was evaluated **(Figure S3, Supporting Information)**, showing an overexpression of *SOX2* and *NANOG* in the VMM15 cell cultures when compared to hDFbs, hDMECs and hASCs. This suggests that VMM15 melanoma cells express high levels of these stemness-related genes, which to the best of our knowledge, is the first time such has been reported. We then questioned whether the expression of these genes would continue to appear upregulated in the multicellular models. Interestingly, we verified higher expression levels of *SOX2*, POU5F1 and *NANOG* in conditions which included the VMM15 melanoma cells (Fig. 3a)**(Figure S4, Supporting Information)**. This pattern of expression was seen for all the 3 genes, with the VMM15 assembloid and the VMM15/hDFbs spheroids showing significant overexpression when compared to the remaining conditions. This is supported by previous studies showing higher expression of *POU5F1, NANOG*, and *SOX2* mRNA transcripts within tumor cells and cancer stem cells niches when compared to those of nontumor tissues [35–37]. When considering the CTRL MCS, where all of the cell constituents were added at the same time, lower levels of expression were observed for SOX2 and NANOG when compared to the remaining VMM15 conditions, which may ultimately be a consequence of the cellular interactions established within the different spheroid compartments beforehand.

We then evaluated at the transcriptional level the abundance of the NAD-Dependent Protein Deacetylase Sirtuin-1 (SIRT1) (Fig. 3a)**(Figure S4, Supporting Information)**, which is physiologically regulated to coordinate responses to environmental stimuli and stressors. More recently, its expression was shown to be elevated in metastatic melanoma when compared with primary melanoma while also being linked to the induction of epithelial–mesenchymal transition (EMT), facilitating melanoma metastasis [38]. Here, *SIRT1* was shown to be underexpressed in the individual MCSs domains ($p < 0.05$) when compared with both of the produced assembloids and the larger CTRL MCS. Taking in account that spheroid size and variability of response to 3D culture have a direct impact on both viability and growth kinetics of cells, which may generate spheroid core necrosis, hypoxia-induced cellular responses and genomic instability [39], we analyzed the mRNA expression of *TINF2* and *TERF2* (Fig. 3a)**(Figure S4, Supporting Information)**. These proteins are part of the shelterin complex, that is composed of six major proteins which are responsible for protecting the telomeric DNA from damages [40]. Higher expression levels of both these genes was evident in conditions comprising the VMM15 melanoma cell line, whereas a significant decrease in the expression of these genes was found in hDMECs/hDFBs ($p < 0.05$ and $p < 0.01$). Also involved in damaged DNA repair is BRCA1, which has been shown to be involved in the repair of double-strand breaks and initiate homologous recombination (HR), linking the maintenance of genomic integrity to tumor suppression [41]. While no statistical difference was found, a trend of underexpression of BRCA1 was noticed in all the studied conditions when compared to the VMM15/hDFbs MCSs, especially for the VMM15 assembloid together with the CTRL MCS (Fig. 3b). Besides BRCA1, TP53BP1 plays a significant role in DNA damage response, promoting checkpoint signaling following DNA damage [42,43]. Once again, no statistically significant differences were observed between condition, despite VMM15/hDMECs MCSs having presented slightly inferior expression values when compared to the remaining conditions (Fig. 3b).

While stemness transcription factors like SOX2, NANOG and POU5F1 are deeply associated to the mesenchymal phenotype in EMT [44], changes in the expression of key players such as E and N–Cadherin (CDH1 and CDH2 respectively), Vimentin (VIM) and Zinc finger E-box binding homeobox 1 (ZEB1) are crucial for cell detachment and tumor metastasization [45]. By assessing the expression profile of these genes within the proposed tumor models we hoped to shed additional light into the cellular interactions occurring within the system. While no statistical differences among the studies conditions were observed, a clear trend towards higher expression of mesenchymal associated genes *ZEB1, CDH2* and *VIM* were observed in the VMM15 assembloid.

The aforementioned results demonstrate that the co-culture of tumor stromal compartments in the form of MCSs allowed for their complete fusion followed by their auto-organization into multilayered 3D cell models. These higher complexity models preserved a gene expression profile compatible with metastatic melanoma, which was already observed for simpler MCSs containing VMM15.

3.3. Tumor assembloids as alternative drug screening tools

Whether a 3D cancer model is capable of responding in vitro to known pharmaceuticals defines how well these systems can mimic in vivo cellular behavior and therefore how effective they are as disease models. Doxorubicin (Dox) was chosen due to its wide use as a chemotherapeutic agent recommended for the treatment of several tumors [46]. Regarding spheroid morphology (Fig. 4a) **(Figure S5, Supporting Information)**, a clear shedding of the most superficial cells was noticed in all conditions in which VMM15 melanoma cells were present. This outer part was previously shown, in the tumor assembloid, to overlap with the location of $GP100^{+}$ VMM15 tumor cells. This shedding was not visible in the CTRL assembloid lacking these tumor cells (Fig. 4a). In both VMM15 conditions, assembloid and CTRL MCS, the shedding was followed by an increase in the spheroid area in comparison to the non-treated condition (Fig. 4b), which is likely a consequence of cell death and detachment. In contrast, the CTRL assembloid didn't present any changes do its area over time when treated with Dox. To validate the potential use of our developed assembloid system for drug screening, a lactate dehydrogenase (LDH) assay was conducted after exposure of the models to 40 μM Dox over 4 days. LDH release in response to Dox (Fig. 4c)**(Figure S6, Supporting Information)** varied for all conditions, albeit conditions comprising the VMM15 melanoma cell line presented overall higher values as expected. The VMM15 assembloid condition was shown to be the most susceptible to Dox (78.89% of the LDH release of the positive

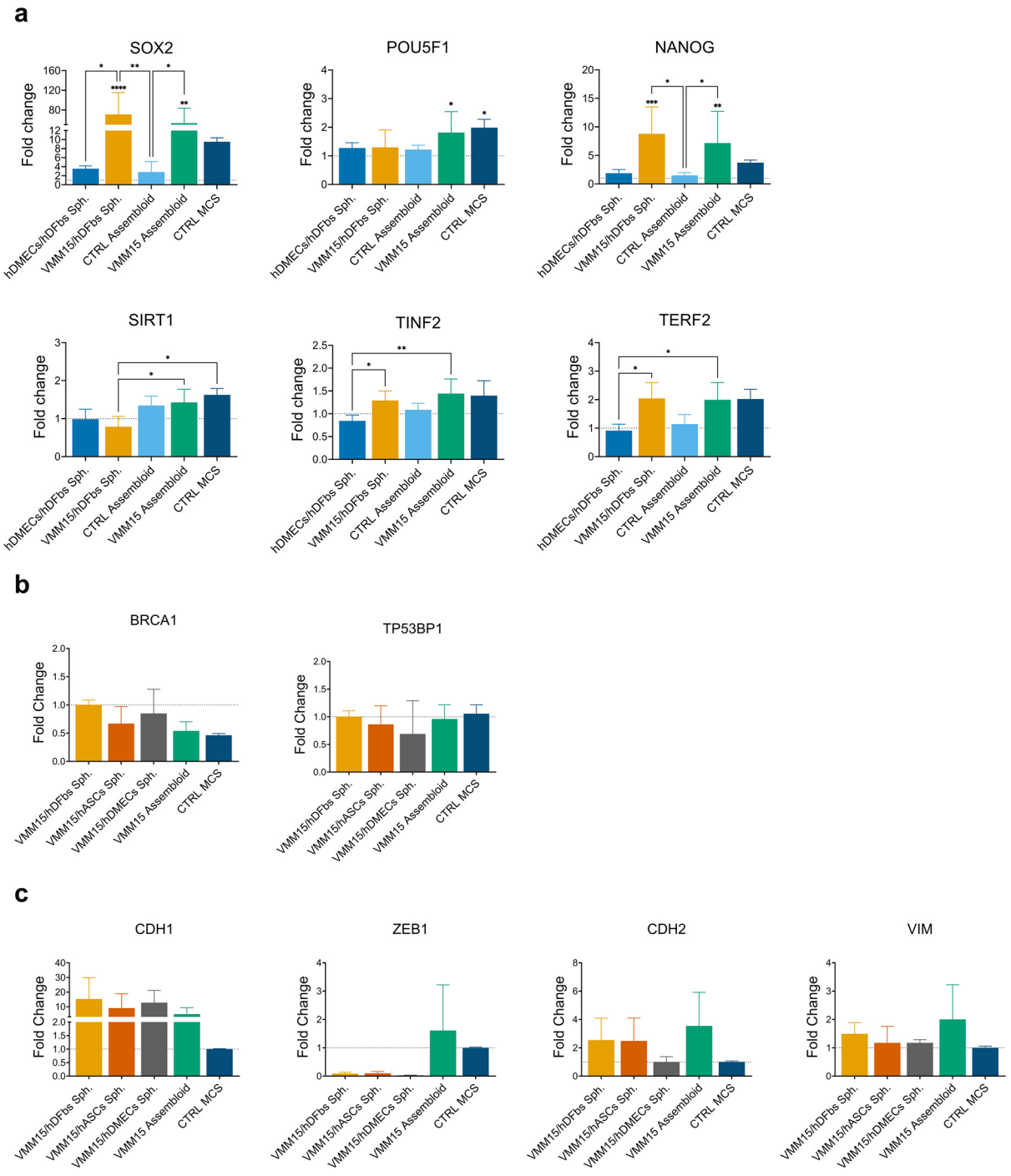


Fig. 3. Phenotypic characterization of assembloids and of their forming subunits. a) *SOX2, POUF5F1, NANOG, SIRT1, TINF2* and *TERF2* mRNA expression in MCSs subdomains, developed assembloids and CTRL MCS at 13 d of total culture. Expression was determined by qPCR using *β2M* as a reference gene and normalized to the hDMECs/hASCs MCSs. b) *BRCA1* and *TP53BP1* mRNA expression in MCSs subdomains, developed assembloids comprising VMM15 melanoma cells and CTRL MCS at 13 d of total culture. Expression was determined by qPCR using *β2M* as a reference gene and normalized to the VMM15/hDFbs MCSs c) *CDH1, ZEB1, CDH2* and *VIM* mRNA expression in MCSs subdomains, developed assembloids comprising VMM15 melanoma cells and CTRL MCS at 13 d of total culture. Expression was determined by qPCR using *β2M* as a reference gene and normalized to the VMM15/hDFbs MCSs. Quantitative results are expressed as the mean ± standard deviation where $n = 3$. When pairwise comparisons are not directly represented, statistical significance is represented by * $p < 0.05$, ** $p < 0.01$, *** $p < 0.001$, **** $p < 0.0001$ when compared to hDMECs/hASCs, after a one-way ANOVA with Kruskal–Wallis multiple comparison post-test.

control) followed by the CTRL MCS (72.56%) and the VMM15/hDFbs spheroid (59.36% LDH release), while hDMECs/hDFbs (34.73%) and hDMECs/hASCs (29.36%) showed significantly lower values. All of these results suggest that our final melanoma assembloid system acted as a responder to Dox, suggesting its suitability as a drug screening platform for further studies.

3.4. Stromal cells and 3D tumor cell invasion in the melanoma assembloid

Cellular interplay and crosstalk within the tumor microenvironment plays a role in promoting tumor growth, maintenance and invasion [47], in part through the activation of several ECM

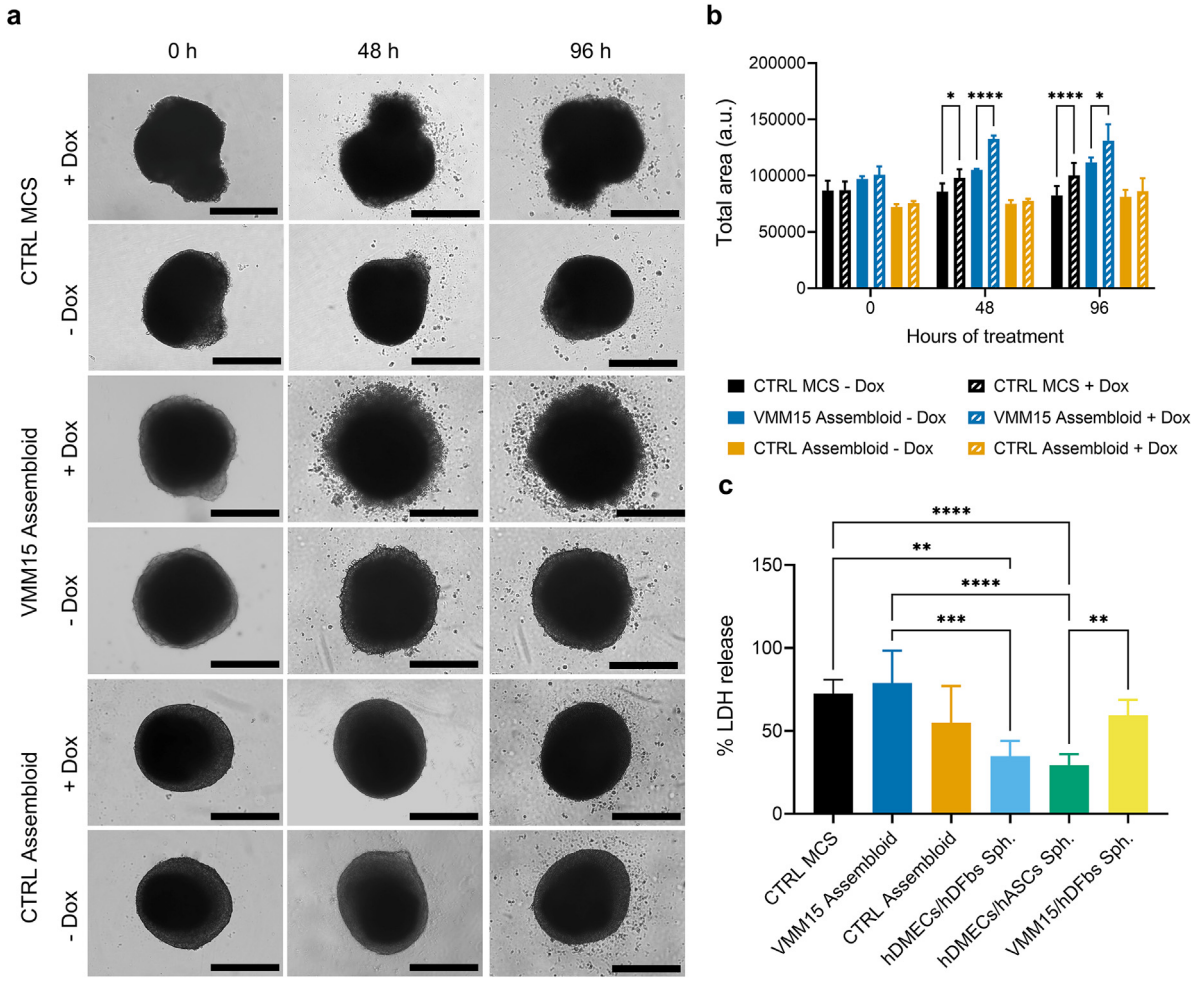


Fig. 4. Characterization of assembloid and CTRL MCS morphology and viability in response to doxorubicin treatment. a) Growth phenotype of melanoma assembloid and controls when stimulated with 40 μM of Dox. Scale bar = 500 µm. b) Total area of VMM15 assembloids and respective controls over time when treated with 40 μM of Dox. c) Cytotoxicity evaluation by LDH release from three independent experiments of VMM15 assembloids, CTRL assembloids and CTRL MCSs exposed to Dox at 40 μM. Quantitative results are expressed as the mean ± standard deviation where $n = 3$. * $p < 0.05$, ** $p < 0.01$, *** $p < 0.001$, **** $p < 0.0001$, one-way ANOVA with Kruskal–Wallis multiple comparison post-test.

degrading MMPs. In melanoma, in particular, a critical role has been attributed to tumor stromal cells and the MMPs they produce in the promotion of tumor invasion [48,49]. Studies have shown that MMP-2 is constitutively expressed with variations implicating modest up or downregulations [50] while MMP-9 expression is highly inducible under the control of growth factors, chemokines and other stimulatory signals [51]. We proceeded in measuring the bioactivity of MMP-2 and MMP-9 in the developed spheroid models (Fig. 5b) **(Figure S7 and S8, Supporting Information)**. Results showed that pro-MMP-2 activity was detected throughout all conditions, with no significant differences found. In the single spheroid model where VMM15 was co-cultured with hDFbs, little to no MMP-2 activity was detected, with the hDMECs/hASCs having in comparison significantly increased activity ($p < 0.05$) of that enzyme over the whole culture period. Significantly higher activity of MMP-2 ($p < 0.05$) was further found in both tested assembloid models when compared to the VMM15/hDFbs spheroid. Expression of active MMP-9 was not detected throughout the tested conditions. Nonetheless, pro-MMP-9 activity was found to be significantly greater in the control assembloid in comparison to VMM15 co-cultured spheroids **(Figure S7, Supporting Information)**. These results suggest that endothelial and stromal cross-talk is important for MMP's, especially MMP-2, activity. While the constitutive gene expression of MMP is low, their expression is regulated at both the transcriptional and post-transcriptional levels. At a post-transcriptional level, the activity of these enzymes is controlled by specific protease inhibitors such as the tissue inhibitors of metalloproteinases (TIMPs). Findings have pointed to TIMP1 and −3 associating with latent or pro-MMP9 while TIMP2, −3 and −4 are capable of interaction with pro-MMP-2 [52]. This considered, we were interested in understanding whether the differences seen in MMP-2 and MMP-9 activation in our developed spheroid models were being mediated by TIMP-1 and TIMP-2. ELISA (Fig. 5c) **(Figure S9, Supporting Information)** assays showed that TIMP-2 production was similar for all conditions with exception to the VMM15/hDFbs MCSs. Regarding TIMP-1, higher levels of this inhibitor were observed for both assembloid conditions and hDMECs/hASCs MCSs in comparison to the remaining MCSs.

This differential expression suggests that the activity of TIMPs is linked to the different stromal cells comprising the tumor microenvironment, therefore highlighting their importance in the development of heterotypic tumor models.

We then investigated whether differences in the production of MMPs would impact overall invasion potential of the different models. We conducted a Matrigel®-based assay to evaluate both the sprouting and the invasion capability of the melanoma assembloids (Fig. 5a) after which spheroid segmentation was performed for further image analysis of migration profiles (Fig. 6a). Three pa-

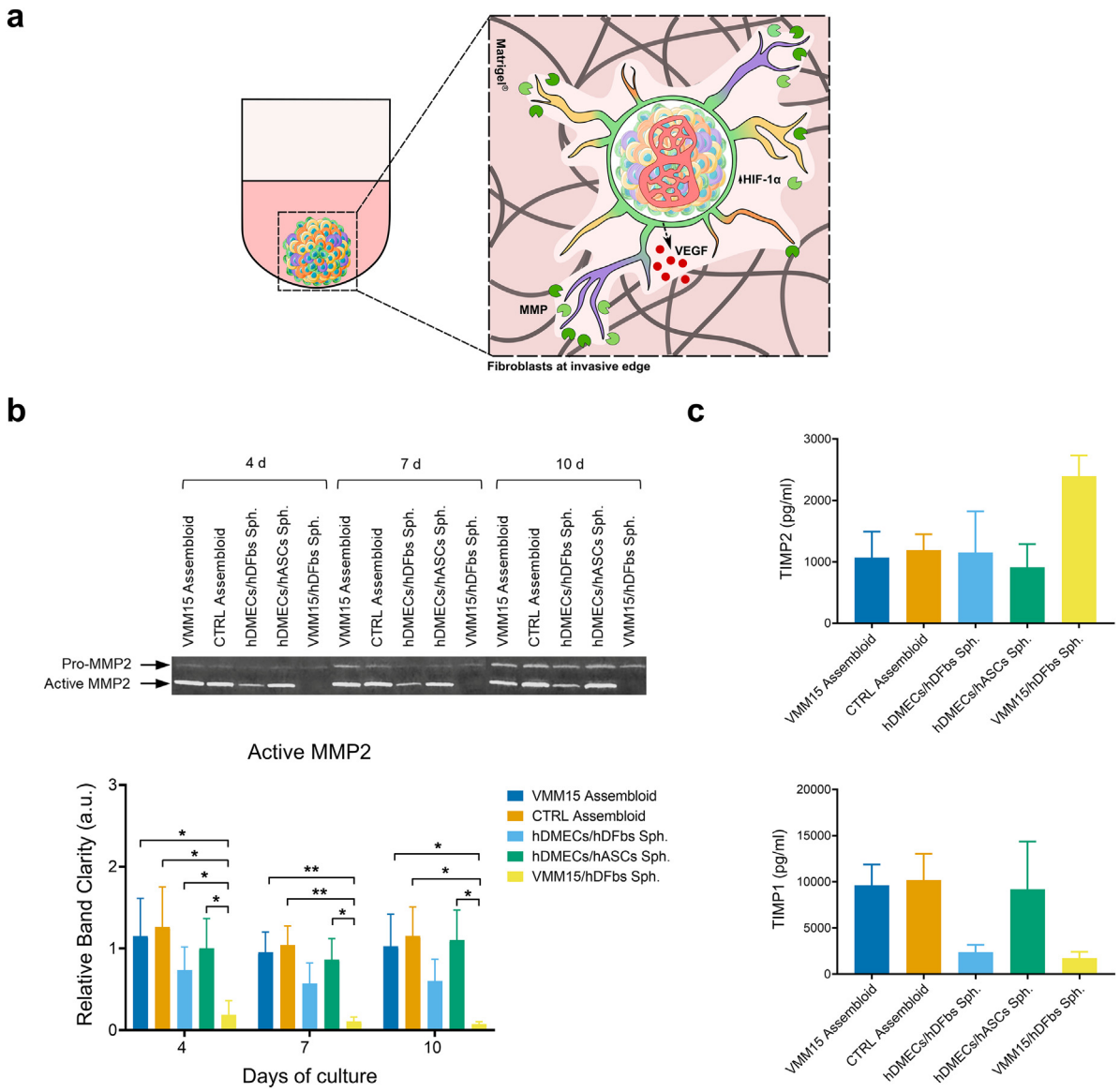


Fig. 5. MMPs as an active agent in melanoma tumor invasion. a) Schematic illustration of tumor assembloid invasion within a 3D Matrigel® assay: a single tumor spheroid per well was embedded in Matrigel®. b) Gelatin zymography of MCSs or assembloid culture medium over 13 d of culture. MMP activity was visualized as clear bands against a dark blue background of gelatin substrate in gel. Molecular weight markers were used to estimate the molecular masses of the pro and active forms of MMP-2. Density of each band expressed as an arbitrary unit. c) *TIMP1* and *TIMP2* secretion in MCSs subdomains and developed assembloids at 13 d of total culture. Expression was determined by ELISA. TIMP-1 was quantified in 5 μg of total protein and TIMP-2 was assessed in 20 μg of total protein. Quantitative results are expressed as the mean ± standard deviation where $n = 3$. * $p < 0.05$, ** $p < 0.01$, *** $p < 0.001$, **** $p < 0.0001$, one-way ANOVA with Kruskal–Wallis multiple comparison post-test.

rameters considered relevant in terms of cellular invasion were assessed: area of invasion, the area of the core and the maximum radius [25]. While an increase in core size was detected for all tested conditions over the 7-day culture period, the greatest significant changes ($p < 0.001$) observed were among the different tumor single spheroids. No decreases in core size were in fact observed in any condition **(Figure S10, Supporting Information)**, suggesting that no necrosis was occurring over the 7-day culture period. However, the CTRL MCS displayed the lowest change in core size dynamics, suggesting hampered proliferative capacity of the cells in this group. The maximum radius is defined as the farthest distance on invasion from the center of the spheroid. When looking at these data for 7 days (Fig. 6b) **(Figure S10, Supporting Information)**, we observed that the spheroids of hDMECs/hDFbs presented the highest invasion distance of 2.54 times the core radius at day 0, followed by the CTRL assembloid at 2.18, the melanoma assembloid at 2.06-fold and the CTRL MCS at 2.04-fold. Interestingly, all the tumor single MCSs presented no visible invasion in the 3D matrices. When performing multiple comparisons among the different conditions in each timepoint, we observed that the single MCSs of VMM15 presented a significantly inferior radius of invasion when compared to the remaining conditions while the co-culture MCS of hDMECs/hDFbs showed the maximum radius of invasion of all conditions **(Figure S10, Supporting Information).**

When studying invasion, not only is the radius of invasion relevant but also the area of the invading edge, which consists in the area occupied by the expanding cellular mass. After 7 days of culture, the role that cross-talk among different stromal cells partakes in invasion area was clear. Single MCSs of VMM15 tumor cells co-cultured with either hDFbs, hASCs or hDMECs presented significantly less invasive potential when directly compared to all the remaining conditions (Fig. 6c) **(Figure S10, Supporting Information)**. The co-culture of hDMECs/hDFbs showed to contribute greatly to the invasive capacity of the spheroid, while the melanoma assem-

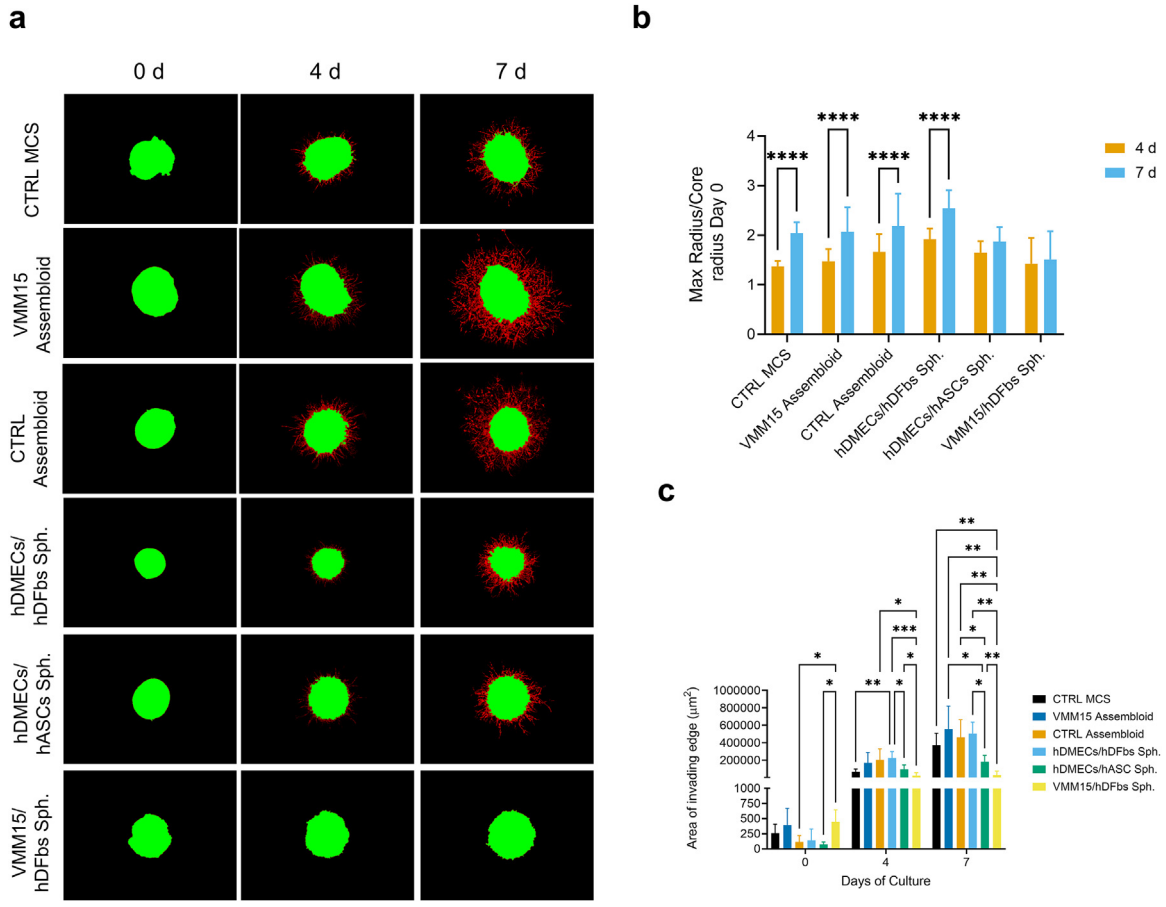


Fig. 6. 3D invasion profile of assembloids and MCSs in Matrigel®. a) Segmentation profiles of MCSs and assembloid invasion in Matrigel® over 7 d (Green= Core; Red = Invasive Edge). (b) Calculation of invasion as a function of the longest invasive distance emanating from the spheroid normalized to core radius at day 0 of the experiment. (c) Calculation of invasion as a function of the area of the invading edge. Scale bar = 200 µm. Quantitative results are expressed as the mean ± standard deviation where $n = 3$. * $p < 0.05$, ** $p < 0.01$, *** $p < 0.001$, **** $p < 0.0001$, one-way ANOVA with Kruskal–Wallis multiple comparison post-test. (For interpretation of the references to color in this figure legend, the reader is referred to the web version of this article.)

bloid comprising all of the 4 different stromal cells showed the highest area of invasion.

We then proceeded to characterize the invasion front namely in terms of the presence of VMM15 cells. For this, GP100 immunolabelling was performed in the 3D matrix used for the invasion assays (Fig. 7)**(Figure S11, Supporting Information)**. Interestingly, GP100-positive cells were found not leading but following the leading edge of the invasion front. Although the presence of randomly detached GP100-positive cells cannot be completely ruled out, results allow the possibility that stromal cells remodel the adjacent ECM to facilitate the migration of the tumor cells following in their wake, as described before [53].

4. Discussion and conclusion

Over the past decade researchers have kept on pushing the boundaries of more traditional 3D cancer models like spheroids, MCSs and organoids. While these systems have made great advances in order to better represent native tissues they still present concerns of their own. Hybrid systems which combine different models together, like the ones reported by Boulard and colleagues [5], bridge the gap between cell-sheet systems and spheroids while capable of presenting a stratified epidermis, a basement membrane and blood and lymphatic capillaries in the engineered tissue. Similarly, organotypic models for melanoma have also been generated [54].

Recently, assembloids were proposed as advanced 3D tissue models with added complexity. Originally envisioned to better study the assembly of neural circuits through the combination of organoids representing multiple brain regions, this form of 3D model allows deeper insights into tissue function, opening doors for the development of more advanced and representative cancer models [55] that will allow for a greater understanding of this disease.

The present work, provides the groundwork to unravel cell-cell and cell-ECM interactions relevant for cancer growth and invasiveness, at different stages of cancer development. Different stromal MCSs were developed to represent different stromal subdomains. Supporting this rationale was the intent of first establishing a stable endothelial cell compartment, capable of acting as a surrogate capillary bed and then combining this with a tumor-like stroma compartment encompassing VMM15 melanoma cells and hDFbs. This allowed the critical interactions between tumor and endothelial cells to take place upon combination of the MCSs into the assembloid system. While in this study we have opted for the use of the VMM15 melanoma cells, various tumor cell lines, whether they have different driver mutations or not, may benefit from this system. However, driver mutations affecting spheroid-forming capabilities of the cells will compromise the use of this method (as demonstrated by Ogishima et al. 2018 [56]).

Given the importance of stromal ECM, the collagen signature in these stromal subdomains was analyzed. The spatial organization of the hDMECs appeared to be coincident with the collagen deposi-

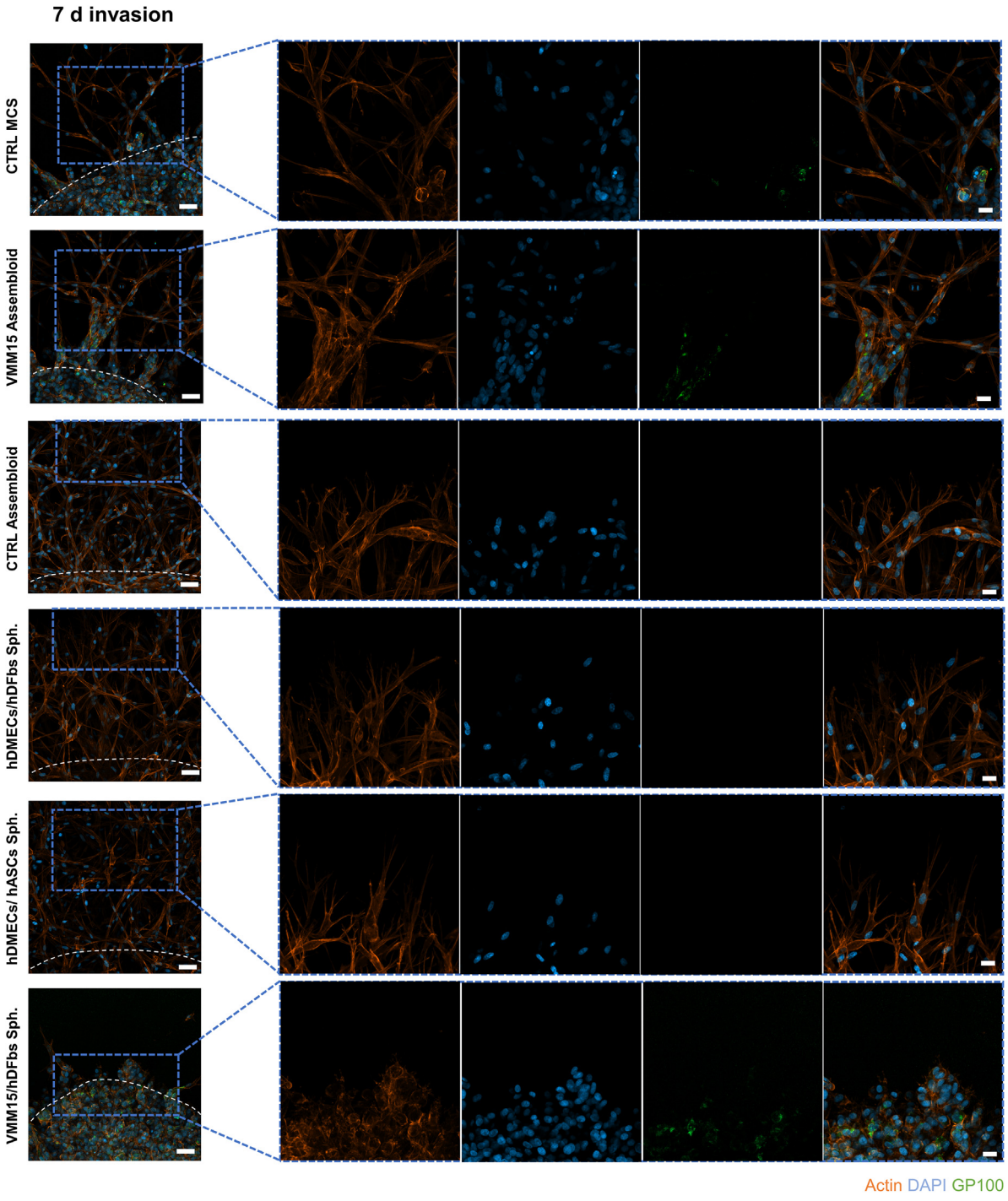


Fig. 7. Invasive migratory behavior of assembloids and MCSs. Details of invadopodia of invading spheroids advancing into the matrix after immunofluorescent labelling, at 7 days of invasion. GP100^{+} melanoma cells are found in green. Nuclei were counterstained with DAPI and cell cytoskeleton with Phalloidin-TRITC. White dashed lines delimit the original bulk of the spheroids. Scale bar = 50 µm (left) and 20 µm (right). (For interpretation of the references to color in this figure legend, the reader is referred to the web version of this article.)

tion seen by PSR staining, which is supported by the demonstrated role of collagen type-1 in endothelial cell morphogenesis [57]. Interestingly, while both fibroblasts and MSCs are known to support vasculogenesis through ECM deposition and secretion of pro-angiogenic factors [58–60] only in the hDFbs-contaning MCS were the hDMECs organized into highly dense vascular-like network. These results are supported by reports showing that fibroblast-derived ECM favors endothelial tubulogenesis [61], while the direct co-culture between MSC and ECs has been shown to potently decrease EC proliferation and their angiogenic potential which may occur via VE-cadherin/β-catenin interactions at the EC cell surface [62].

When the individual MCSs where assembled together, spatial organization of the different cells types in layers was evident at 10 days of combinatorial culture. Within this layered structure endothelial cells migrated toward the core of the spheroid, fibroblasts and stem cells remained in the central senescent zone and the VMM15 tumor cells migrated towards the outward prolifer-

ating zone. This organization comes in agreement with the cellular arrangement observed in other melanoma models [63], where growth factor deprivation, nutrients and oxygen gradients, and catabolites accumulation are responsible for segregating melanoma cells into a continuously proliferating subpopulation in the periphery and a G1-arrested subpopulation in the center [63]. This is similar to what is verified in vivo where tumor growth is characterized by a phase of exponential cell proliferation followed by a phase of declining growth rate associated with an increase in nonproliferating (quiescent) cells and necrotic cells [64]. This form of hierarchical organization was shown to be size dependent, in which MCS larger than 500 μm in diameter present a necrotic core surrounded by a viable rim, with an inner layer of quiescent cells and an outer layer of proliferating cells [65]. It is worth adding that among the different subtypes of melanoma, Vertical Growth Phase (VGP), is characterized by deep vertical growth into the tissue with while displaying invasive and metastatic properties [66,67]. In this melanoma subtype, nests become ever so smaller until, eventually, single melanocytes can be found coursing individually through the dermis. In histopathological terms [67], this comes in agreement with our VMM15 assembloid in which the tumor cells are not strictly confined within a spherical structure.

While comprising the same cellular constituents, the CTRL MCS failed to present a visible organization. GP100$^+$ cells were irregularly distributed in the outermost layer of the spheroid and cell bulging and loose cell aggregates were frequently present. The poor spatial organization of hDFbs, hDMECs and hASCs may be related to the observed diminished collagen deposition. A previous report had already observed that when endothelial cells were seeded together with fibroblasts and tumor cells on day one, no endothelial cells were located in the microtissues [68], which comes in agreement with our results in regards to the lack of CD31$^+$ cells within the CTRL MCS. This comes to show that the establishment of stromal compartments, followed by their assembly into a more complex structure such as what is herein proposed, supports the viability and function of these stromal cells.

Also deemed critical for this hierarchical organization is the deposition of ECM within these 3D models, which relays both biochemical and physical stimuli affecting all surrounding cells in terms of cell migration, differentiation, proliferation and viability [69,70]. This form of support and biochemical stimulation provided by the different cellular subsets may explain the fast fusion of the individual sub-domains into one larger assembloid when placed in co-culture. The 28-day total culture period resulted in extensive necrosis at the core of the tumor assembloid when compared to the CTRL condition. It is possible that this occurred not only in function of the size of the assembloid but equally because of the dense ring of VMM15 cells that had formed around it, this way shielding the inner cells from nutrients and oxygen, which has been shown to occur in vivo [64]. These VMM15 cells also presented Ki-67 expression at 13 days of total culture which correlates with what has been observed in several studies in which it was shown that the expression of this proliferation marker was known to be higher in tumor stromal areas of metastases and in tumor cell areas of primary tumors while also being associated with tumor grade and pathological nodal involvement [71–73].

The role that cancer stem cells, a subpopulation of tumor cells which display stem cell features, plays within the tumor microenvironment has become of high importance in understanding the mechanisms behind tumor invasiveness, metastasis, drug resistance and epithelial to mesenchymal transition (EMT) [74]. Tightly associated to this phenotype is the overexpression of pluripotency transcription factors *SOX2, POU5F1* and *NANOG* which have been reported to induce stemness, chemoresistance, metastatic potential, proliferation, EMT and resistance to apoptosis and are directly tied to aggressiveness and poor prognosis [75–78]. We have shown that the VMM15 melanoma cell line displays such features in light of its overexpression of pluripotency transcription factors *SOX2* and *NANOG* in 2D monocultures. Similarly, the overexpression of these transcription factors was verified both in our melanoma assembloid model, within the individual MCSs comprising VMM15 cells as well as in the CTRL MCS albeit in an inferior manner in the latter. This suggests that the 3D culture supported the maintenance of this stemness profile. Tumor cells have also been shown to promote the upregulation of these stemness related genes in neighbor cells as the case of hASCs [79]. Additionally, overexpression of *POU5F1* was only verified in the 3D conditions which may be an effect of the heterogeneity of the neighboring cells which impacts cytokine levels, hypoxia, acidic pH, cancer associated fibroblasts (CAFs) and the activation of specific signaling pathways which are known to regulate cancer stem cell niches [80].

While the role of SIRT may vary between tumor suppression and tumor promotion depending on the signaling pathway or targets involved, its expression has been shown to be increased in melanoma and has been associated as a marker of bad prognosis [38,81,82]. Beyond its association to proliferation and cancer cell growth, studies have also linked the overexpression of SIRT-1 to the enhanced the expression of the mesenchymal marker's vimentin and N-cadherin [76]. Within our results we have shown that both the VMM15 assembloid and the CTRL MCS present the highest levels of *SIRT1* that in turn correlates with EMT promotion. These higher levels were also coincident with the enhanced expression of *ZEB1, CDH2* and *VIM* in the VMM15, suggesting a possible connection between both signaling pathways in this model. Also associated with several roles in cancer is the shelterin complex [83]. While protecting the telomere from DNA damage pathways and aging, it may act as an oncogene in cancer cells. An overexpression of the *TINF2* and *TERF2* genes has been implicated in various pro-tumorigenic mechanisms [84]. Our results are in line with these findings, where an increased expression of these genes was detected in VMM15 cells-bearing spheroids and in the melanoma assembloid. Genomic instability in our models was further studied by assessing the expression of *BRCA1* and *TP53BP1* genes. Both *BRCA1* and *TP53BP1* have been indicated as tumor suppressor genes with important roles in DNA damage repair. A loss of expression of *BRCA1* has been shown to lead to a higher tumor grade and advanced clinical stage in gastric carcinoma patients [85], while in breast cancer tissues a decrease in *BRCA1* levels led to tumor cell growth while an increase in its expression triggered growth arrest and apoptosis [86]. A similar behavior is observed with *TP53BP1* in which loss of protein expression levels were associated with high grade tumors, supporting the idea that loss of function of this gene may favor breast cancer progression and worse prognosis [87]. In patients with pancreatic ductal adenocarcinoma, loss of *TP53BP1* expression was also associated with decreased overall survival [88]. Our results suggest a trend for underexpression of *BRCA1* for the assembloid model together with the CTRL MCS in comparison with most MCSs conditions, indicating the genomic instability typical of higher-grade tumors is preserved in this complex model. The seemingly opposing trends of expression found in the developed melanoma model are not totally unexpected. While BRCA1 and TP53BP1 are both involved in DNA damage repair, they present different means of action. BRCA1 promotes DNA end resection and homologous recombination (HR) during S/G 2 phases of the cell cycle and while TP53Bp1 inhibits end resection and facilitates non-homologous end-joining (NHeJ) primarily during G1 [89]. Studies on these competitive methods of DNA damage repair show that TP53BP1 may in fact act as an inhibitor of BRCA1 accumulation at double-strand break sites [90]. An alternative explanation for the observed opposing trends of expression may be related to BRCA1-deficient cells [91]. This phenotype has been associated to several different tumors namely, ovar-

ian carcinoma, prostate cancer and mammary tumors [92–94]. Further assays specifically studying the mechanisms behind double-strand DNA repair in our system are needed for a full clarification of the observed results. "Classical" EMT is a biological process involved in embryogenesis and organ development [95] and has been deemed critical for several distinct pathologies such as chronic inflammation and cancer [96–98]. In EMT, polarized epithelial cells undergo a phenotypic switch into a mesenchymal cell phenotype [99] which is defined by a decrease in the expression of the epithelial marker E-cadherin [100–102] followed by an increase in the expression of N-cadherin [103–105]. During this switch, cells acquire enhanced migratory capacity, invasiveness, greater resistance to apoptosis, and increased production of ECM components [99]. This mechanism in regulated by a series of EMT–activating transcription factors such as those from the SNAI, ZEB and TWIST families. However, it is important to highlight that their role in promoting EMT is rather complicated considering that their functions are often non-redundant and tissue-specific. Studies such as the one performed by Caramel et al. show that in metastatic melanoma, the EMT transcription factor network undergoes a reorganization in favor of TWIST1 and ZEB1 [106]. In our proposed VMM15 assembloid model, we could observe a trend towards higher expression of this transcription factor when compared to the remaining conditions comprising VMM15 tumor cells in their composition. Interestingly, a trend for higher expression of *CDH2* and *VIM* was also observed for this condition. Previous studies have indeed shown as increased expression of these two molecules in melanoma [8,104,107,108]. The role that fibroblasts undertake in controlling these processes is also worth mentioning. Different fibroblasts phenotypes were shown to induce different activation statuses of G361 melanoma cells while inducing higher expression levels of *CDH1* and *CDH2* genes [8]. When discussing EMT in cancer tissues, its deep association to the concept of cancer stem cells cannot be ignored. Reports have addressed the fact that EMT can induce cancer cell stemness in distinct tissues [109] while several EMT-related transcription factors have displayed the capacity to promote cancer stem cell stemness in human breast cancer models [110]. Nonetheless, while an insight on the biological changes that are occurring in the studied systems can be uncovered to an extent through the use of technologies like real-time PCR to analyze gene expression profiles, one must be cautious in discussing these results as the observed gene expression signatures are not of specific cell types within the spheroid but of the system as whole. It is nevertheless likely that the changes described in the results above are more or less pronounced depending on the studied cell population of the models proposed. Single cell analysis or spatial transcriptomics would allow a more detailed characterization of the changes happening during the different stages of the study, which is a limitation of the current work.

The reaction of 3D tumor models to anti-cancer agents is of key interest to assess its potential to mimic what happens in vivo and be used for drug discovery. A higher sensitivity to Dox was observed in conditions comprising VMM15 melanoma cells correlating with increased cell shedding in the assembloid and MCSs and an increased LDH release. This increased sensitivity may be consequence of the cellular organization seen in this model where VMM15 tumor cells are in the proliferative zone and therefore in first contact with the drug while these cells' higher proliferation rate makes them more susceptible to apoptosis by DNA damage. It is crucial to highlight that while the observed differences between the VMM15 assembloids and the VMM15/hDFbs spheroid were not statistically significant and therefore may appear to fall short, our new platform was able to maintain its responsiveness to an anti-cancer agent while adding a significant layer of complexity and heterogeneity and proving the applicability of this system for drug screening purposes. Furthermore, this structured organization present in the assembloid has the potential to facilitate the unravelling of the mechanisms leading to anti-cancer therapeutic resistance in tumors [111,112] by studying cell-cell interactions within layer interfaces.

Having observed a complete overhaul in cellular organization of the 3 stromal subdomains when assembled, we questioned how this would impact cell invasion in 3D. Cellular crosstalk and paracrine signaling in the tumor microenvironment are key to drive tumor progression [113–115]. Among the major players involved, we can find MMPs which are a family of zinc-containing endopeptidases, similar between themselves both structurally and functionally. They are secreted in an inactive (latent) state, known as pro-MMPs, and require activation in order to be able to cleave ECM components [116] while their activity appears to be tightly regulated by TIMP function. Whereas MMPs are known for their important physiological functions such as tissue repair and remodeling, cellular differentiation, cell mobility and wound healing [117], gelatinases (MMP-2 and MMP-9) in particular have been implicated as key players in promoting angiogenesis, infiltration of cancer cells and metastasis [118–120]. Active MMP-2, in particular, was shown to correlate with increased malignancy in melanoma xenograft models [49], as well as in primary and metastatic melanoma patients [121]. Endothelial cells have a clear role in this mechanism through which the spread of tumor cells throughout the capillary endothelium and neovascularization are facilitated [122,123]. This effect seems present when comparing the results of MMP activity in the matrix-embedded cultures. An increased production of active MMP-2 was visible in conditions that presented a higher invasive area and maximum length of invasive edge from the spheroid core, that mostly coincided with the presence of hDMECs and hDFbs combinations. Interestingly, co-culture MCS containing VMM15 cancer cells all presented relatively low levels of MMP production and invasion, independently of being cultured with endothelial cells, mesenchymal stem cells or fibroblasts. In humans, an inverse relationship between in situ MMP-9 expression and melanoma progression was found [124]. MMP-9 appears to be involved in the early steps of metastasis formation but not the later steps such as extravasation [125]. In most cases of tumor development and progression, MMPs are produced by nonmalignant stromal cells within the tumor microenvironment. Besides the known production of these gelatinases by endothelial cells, findings have pointed to the production of MMPs to be associated to fibroblasts immediately surrounding tumor cell clusters [126,127]. This adds to the importance of having heterotypic cellular models in which crosstalk between different stomal cells is allowed, mimicking the in vivo situation and specific phenomena such as "cooperative invasion". The latter describes how inherently invasive cells, either malignant or nonmalignant, can induce the invasion of otherwise poorly invasive subpopulations in mixed cell populations [128]. Several mechanisms supporting this concept have been described. One in particular describes an invasive or leader cell that possesses protease activity, deposits ECM and co-invades through the 3D matrix with subpopulations of poorly invasive cells [129]. Other reports have supported this concept in melanoma [129–131]. Chapman and colleagues [129], for instance, showed that the co-culture between cells of different invasive potential altered the behavior of the poorly invasive cells into actively invading in the heterogenous environment. In these findings, not only were the highly invasive cells leading the front but also this process was shown to be dependent on MT1-MMP. A similar process may be speculated to occur in our assembloid tumor model, where GP100^{+} VMM15 tumor cells trailed the invasive edge of the produced assembloids. Nonetheless, the role of MMPs in supporting cell invasion in the developed models should be further validated using specific assays. One protocol could involve the addition of a MMP inhibitor such as marimastat, a broad spectrum inhibitor of matrix metallopro-

teases, to the culture system during the invasion assays. Additionally, to confirm the suggested mechanism of cooperative invasion between stromal cells and tumor cells in our 3D tumor model, it would be essential to label each cell population individually, allowing for a clarification of each cell's role in the invasive edge of the assembloid over time. These are limitations of the current work that must be addressed in future implementations of the same assembloid methodology.

While proteases are essential players in invasion, it's actually the balance between proteases and their inhibitors that defines the invasiveness of tumor cells within the microenvironment. Within extracellular fluids and tissues, TIMPs levels have been shown to be in excess when compared to MMPs, thereby limiting their proteolytic activity to focal pericellular sites [132]. The expression of *TIMP1* within tumors correlates with a less aggressive tumor onset while an imbalance in MMP/TIMP ratio seen through the downregulation of *TIMP1* is associated with poor prognosis [133,134]. Additional studies have also pointed to the importance of TIMPs in the reduction of experimental metastasis of melanoma [135]. Our results have shown a correlation between the expression of MMP-2/TIMP-2 and Pro-MMP-9/TIMP-1. Those suggest a possible imbalance in MMP-2/TIMP-2 ratio as seen by the high levels of the active form of MMP-2. On the other hand, TIMP-1 production correlated with the data obtained for pro-MMP-9 through zymography in which no active form of this MMP was present. This may be an indication that an equilibrium in this MMP/TIMP ratio is present, inhibiting therefore the active form of the protease.

Here, we have shown that melanoma assembloids present a hierarchical cellular organization with proliferative and necrotic areas and likely a quiescent are in-between, mimicking native tumor tissue. Sensitivity to Dox was demonstrated. The melanoma assembloid model furthermore favored the overexpression of key pluripotency transcription regulators, which may indicate that this model supports a more dedifferentiated state of the melanoma cells. Moreover, while it is conceivable that the cellular complexity of the model promotes communication among stromal cells, potentially fostering 3D tumor cell invasion through MMP production, as evidenced in other models [128,129,136], further comprehensive studies of the developed models are essential to validate this hypothesis. Furthermore, a finer analysis of cellular and molecular events during assembloid formation, will allow to further unravel the mechanisms behind the observed cellular segregation, which may benefit cancer modelling research and also basic cancer research. In sum, the presented assembloid-based model has the potential to be a powerful alternative to current in vitro 3D tumor models by allowing the study of several melanoma related traits such as anticancer drug sensitivity, pathway plasticity, dedifferentiation and stromal mimicry.

Declaration of competing interest

The authors declare that they have no known competing financial interests or personal relationships that could have appeared to influence the work reported in this paper.

Funding

Authors would like to acknowledge the financial support from the European Research Council through the Starting Grant "CapBed" (ERC-2018-STG-805411), FCT/MCTES (Fundação para a Ciência e a Tecnologia/Ministério da Ciência, Tecnologia, e Ensino Superior) through the grants SFRH/BD/119756/2016 and COVID/BD/151751/2021 (D.B.R.) and to the FSE/POCH (Fundo Social Europeu através do Programa Operacional do Capital Humano) under the scope of the PD/169/2013, NORTE-08-5369-FSE-000037 (H.R.M.). The authors would additionally like to thank the contributions to this work from the project "TERM RES Hub—Scientific Infrastructure for Tissue Engineering and Regenerative Medicine", reference PINFRA/22190/2016 (Norte-01-0145-FEDER-022190), funded by the Portuguese National Science Foundation (FCT) in cooperation with the Northern Portugal Regional Coordination and Development Commission (CCDR-N). Lastly, we would like to equally acknowledge financial support from https://doi.org/10.54499/UIDB/50026/2020; https://doi.org/10.54499/UIDP/50026/2020 and https://doi.org/10.54499/LA/P/0050/2020.

Supplementary materials

Supplementary material associated with this article can be found, in the online version, at doi:10.1016/j.actbio.2024.02.023.

References

[1] National Cancer Institute Melanoma of the Skin-Cancer Stat Facts. [(Accessed 12 July 2022)]; Available online: https://seer.cancer.gov/statfacts/html/melan.html, (n.d.).
[2] R.L. Siegel, K.D. Miller, H.E. Fuchs, A. Jemal, Cancer statistics, 2022, CA Cancer J. Clin. 72 (2022) 7–33, doi:10.3322/caac.21708.
[3] K.I. Votanopoulos, S. Forsythe, H. Sivakumar, A. Mazzocchi, J. Aleman, L. Miller, E. Levine, P. Triozzi, A. Skardal, Model of patient-specific immune-enhanced organoids for immunotherapy screening: feasibility study, Ann. Surg. Oncol. 27 (2020) 1956–1967, doi:10.1245/s10434-019-08143-8.
[4] H. Vörsmann, F. Groeber, H. Walles, S. Busch, S. Beissert, H. Walczak, D. Kulms, Development of a human three-dimensional organotypic skin-melanoma spheroid model for in vitro drug testing, Cell Death. Dis. 4 (2013) e719, doi:10.1038/cddis.2013.249.
[5] J. Bourland, J. Fradette, F.A. Auger, Tissue-engineered 3D melanoma model with blood and lymphatic capillaries for drug development, Sci. Rep. 8 (2018) 13191, doi:10.1038/s41598-018-31502-6.
[6] J. Farhat, I. Pandey, M. AlWahsh, Transcending toward advanced 3D-cell culture modalities: a review about an emerging paradigm in translational oncology, Cells 10 (2021), doi:10.3390/cells10071657.
[7] J. Klicks, C. Maßlo, A. Kluth, R. Rudolf, M. Hafner, A novel spheroid-based co-culture model mimics loss of keratinocyte differentiation, melanoma cell invasion, and drug-induced selection of ABCB5-expressing cells, BMC Cancer 19 (2019) 402, doi:10.1186/s12885-019-5606-4.
[8] J. Novotný, K. Strnadová, B. Dvořánková, Š. Kocourková, R. Jakša, P. Dundr, V. Pačes, K. Smetana, M. Kolář, L. Lacina, Single-cell RNA Sequencing unravels heterogeneity of the stromal niche in cutaneous melanoma heterogeneous spheroids, Cancers 12 (2020), doi:10.3390/cancers12113324.
[9] E.K. Rofstad, A. Wahl, C.de L. Davies, T. Brustad, Growth characteristics of human melanoma multicellular spheroids in liquid-overlay culture: comparisons with the parent tumour Xenografts, Cell Prolif. 19 (1986) 205–216, doi:10.1111/j.1365-2184.1986.tb00731.x.
[10] K. Ramgolam, J. Lauriol, C. Lalou, L. Lauden, L. Michel, P. de la Grange, A.-M. Khatib, F. Aoudjit, D. Charron, C. Alcaide-Loridan, R. Al-Daccak, Melanoma spheroids grown under neural crest cell conditions are highly plastic migratory/invasive tumor cells endowed with immunomodulator function, PLoS ONE 6 (2011) e18784.
[11] G. Cheng, J. Tse, R.K. Jain, L.L. Munn, Micro-environmental mechanical stress controls tumor spheroid size and morphology by suppressing proliferation and inducing apoptosis in cancer cells, PLoS ONE 4 (2009) e4632.
[12] N.K. Haass, K.S.M. Smalley, M. Herlyn, The role of altered cell-cell communication in melanoma progression, J. Mol. Histol. 35 (2004) 309–318, doi:10.1023/b:hijo.0000032362.35354.bb.
[13] N.K. Haass, K.S.M. Smalley, L. Li, M. Herlyn, Adhesion, migration and communication in melanocytes and melanoma, Pigment. Cell Res. 18 (2005) 150–159, doi:10.1111/j.1600-0749.2005.00235.x.
[14] C. Herraiz, C. Jiménez-Cervantes, B. Sánchez-Laorden, J.C. García-Borrón, Functional interplay between secreted ligands and receptors in melanoma, Semin. Cell Dev. Biol. 78 (2018) 73–84, doi:10.1016/j.semcdb.2017.06.021.
[15] Y. Park, C.K. Franz, H. Ryu, H. Luan, K.Y. Cotton, J.U. Kim, T.S. Chung, S. Zhao, A. Vazquez-Guardado, D.S. Yang, K. Li, R. Avila, J.K. Phillips, M.J. Quezada, H. Jang, S.S. Kwak, S.M. Won, K. Kwon, H. Jeong, A.J. Bandodkar, M. Han, H. Zhao, G.R. Osher, H. Wang, K. Lee, Y. Zhang, Y. Huang, J.D. Finan, J.A. Rogers, Three-dimensional, multifunctional neural interfaces for cortical spheroids and engineered assembloids, Sci. Adv. 7 (2021) eabf9153, doi:10.1126/sciadv.abf9153.
[16] C.E. Vorwald, S. Joshee, J.K. Leach, Spatial localization of endothelial cells in heterotypic spheroids influences Notch signaling, J. Mol. Med. 98 (2020) 425–435, doi:10.1007/s00109-020-01883-1.
[17] M. Rausch, L. Blanc, O. De Souza Silva, O. Dormond, A.W. Griffioen, P. Nowak-Sliwinska, Characterization of renal cell carcinoma heterotypic 3D co-cultures with immune cell subsets, Cancers 13 (2021), doi:10.3390/cancers13112551.
[18] J.A. Bagley, D. Reumann, S. Bian, J. Lévi-Strauss, J.A. Knoblich, Fused cerebral organoids model interactions between brain regions, Nat. Methods 14 (2017) 743–751, doi:10.1038/nmeth.4304.

[19] F. Birey, J. Andersen, C.D. Makinson, S. Islam, W. Wei, N. Huber, H.C. Fan, K.R.C. Metzler, G. Panagiotakos, N. Thom, N.A. O'Rourke, L.M. Steinmetz, J.A. Bernstein, J. Hallmayer, J.R. Huguenard, S.P. Paşca, Assembly of functionally integrated human forebrain spheroids, Nature 545 (2017) 54–59, doi:10.1038/nature22330.
[20] Y. Xiang, Y. Tanaka, B. Cakir, B. Patterson, K.-Y. Kim, P. Sun, Y.-J. Kang, M. Zhong, X. Liu, P. Patra, S.-H. Lee, S.M. Weissman, I.-H. Park, hESC-derived thalamic organoids form reciprocal projections when fused with cortical organoids, Cell Stem Cell 24 (2019) 487–497 .e7, doi:10.1016/j.stem.2018.12.015.
[21] S.A. Sloan, J. Andersen, A.M. Paşca, F. Birey, S.P. Paşca, Generation and assembly of human brain region-specific three-dimensional cultures, Nat. Protoc. 13 (2018) 2062–2085, doi:10.1038/s41596-018-0032-7.
[22] R.M. Marton, S.P. Paşca, Organoid and assembloid technologies for investigating cellular crosstalk in human brain development and disease, Trends. Cell Biol. 30 (2020) 133–143, doi:10.1016/j.tcb.2019.11.004.
[23] H. Hama, H. Kurokawa, H. Kawano, R. Ando, T. Shimogori, H. Noda, K. Fukami, A. Sakaue-Sawano, A. Miyawaki, Scale: a chemical approach for fluorescence imaging and reconstruction of transparent mouse brain, Nat. Neurosci. 14 (2011) 1481–1488, doi:10.1038/nn.2928.
[24] J. Schindelin, I. Arganda-Carreras, E. Frise, V. Kaynig, M. Longair, T. Pietzsch, S. Preibisch, C. Rueden, S. Saalfeld, B. Schmid, J.-Y. Tinevez, D.J. White, V. Hartenstein, K. Eliceiri, P. Tomancak, A. Cardona, Fiji: an open-source platform for biological-image analysis, Nat. Methods 9 (2012) 676–682, doi:10.1038/nmeth.2019.
[25] C. Moriconi, V. Palmieri, R. Di Santo, G. Tornillo, M. Papi, G. Pilkington, M. De Spirito, M. Gumbleton, INSIDIA: a FIJI macro delivering high-throughput and high-content spheroid invasion analysis, Biotechnol. J. 12 (2017) 1700140, doi:10.1002/biot.201700140.
[26] J. Dong, J. Grunstein, M. Tejada, F. Peale, G. Frantz, W.-C. Liang, W. Bai, L. Yu, J. Kowalski, X. Liang, G. Fuh, H.-P. Gerber, N. Ferrara, VEGF-null cells require PDGFR alpha signaling-mediated stromal fibroblast recruitment for tumorigenesis, EMBO J. 23 (2004) 2800–2810, doi:10.1038/sj.emboj.7600289.
[27] K.A. Myers, K.T. Applegate, G. Danuser, R.S. Fischer, C.M. Waterman, Distinct ECM mechanosensing pathways regulate microtubule dynamics to control endothelial cell branching morphogenesis, J. Cell Biol. 192 (2011) 321–334, doi:10.1083/jcb.201006009.
[28] J.M. Butler, H. Kobayashi, S. Rafii, Instructive role of the vascular niche in promoting tumour growth and tissue repair by angiocrine factors, Nat. Rev. Cancer 10 (2010) 138–146, doi:10.1038/nrc2791.
[29] I. Cornil, D. Theodorescu, S. Man, M. Herlyn, J. Jambrosic, R.S. Kerbel, Fibroblast cell interactions with human melanoma cells affect tumor cell growth as a function of tumor progression, Proc. Natl. Acad. Sci. 88 (1991) 6028 LP –6032, doi:10.1073/pnas.88.14.6028.
[30] A.E. Karnoub, A.B. Dash, A.P. Vo, A. Sullivan, M.W. Brooks, G.W. Bell, A.L. Richardson, K. Polyak, R. Tubo, R.A. Weinberg, Mesenchymal stem cells within tumour stroma promote breast cancer metastasis, Nature 449 (2007) 557–563, doi:10.1038/nature06188.
[31] S.-M. Han, S.-H. Han, Y.-R. Coh, G. Jang, J. Chan Ra, S.-K. Kang, H.-W. Lee, H.-Y. Youn, Enhanced proliferation and differentiation of Oct4- and Sox2-overexpressing human adipose tissue mesenchymal stem cells, Exp. Mol. Med. 46 (2014) e101–e101, doi:10.1038/emm.2014.28.
[32] M. Pitrone, G. Pizzolanti, L. Tomasello, A. Coppola, L. Morini, G. Pantuso, R. Ficarella, V. Guarnotta, S. Perrini, F. Giorgino, C. Giordano, NANOG plays a hierarchical role in the transcription network regulating the pluripotency and plasticity of adipose tissue-derived stem cells, Int. J. Mol. Sci. 18 (2017) 1107, doi:10.3390/ijms18061107.
[33] I. Ben-Porath, M.W. Thomson, V.J. Carey, R. Ge, G.W. Bell, A. Regev, R.A. Weinberg, An embryonic stem cell-like gene expression signature in poorly differentiated aggressive human tumors, Nat. Genet. 40 (2008) 499–507, doi:10.1038/ng.127.
[34] A.C. Hepburn, R.E. Steele, R. Veeratterapillay, L. Wilson, E.E. Kounatidou, A. Barnard, P. Berry, J.R. Cassidy, M. Moad, A. El-Sherif, L. Gaughan, I.G. Mills, C.N. Robson, R. Heer, Correction: the induction of core pluripotency master regulators in cancers defines poor clinical outcomes and treatment resistance, Oncogene 38 (2019) 4425, doi:10.1038/s41388-019-0826-2.
[35] G. Basati, H. Mohammadpour, A.E. Razavi, Association of high expression levels of SOX2, NANOG, and OCT4 in gastric cancer tumor tissues with progression and poor prognosis, J. Gastrointest. Cancer 51 (2020) 41–47, doi:10.1007/s12029-018-00200-x.
[36] B.W. Kim, H. Cho, C.H. Choi, K. Ylaya, J.-Y. Chung, J.-H. Kim, S.M. Hewitt, Clinical significance of OCT4 and SOX2 protein expression in cervical cancer, BMC. Cancer 15 (2015) 1015, doi:10.1186/s12885-015-2015-1.
[37] S.-H. Chiou, M.-L. Wang, Y.-T. Chou, C.-J. Chen, C.-F. Hong, W.-J. Hsieh, H.-T. Chang, Y.-S. Chen, T.-W. Lin, H.-S. Hsu, C.-W. Wu, Coexpression of Oct4 and Nanog enhances malignancy in lung adenocarcinoma by inducing cancer stem cell-like properties and epithelial-mesenchymal transdifferentiation, Cancer Res. 70 (2010) 10433–10444, doi:10.1158/0008-5472.CAN-10-2638.
[38] T. Sun, L. Jiao, Y. Wang, Y. Yu, L. Ming, SIRT1 induces epithelial-mesenchymal transition by promoting autophagic degradation of E-cadherin in melanoma cells, Cell Death. Dis. 9 (2018) 136, doi:10.1038/s41419-017-0167-4.
[39] S. Riffle, R.N. Pandey, M. Albert, R.S. Hegde, Linking hypoxia, DNA damage and proliferation in multicellular tumor spheroids, BMC. Cancer 17 (2017) 338, doi:10.1186/s12885-017-3319-0.
[40] T. de Lange, Shelterin: the protein complex that shapes and safeguards human telomeres, Genes Dev. 19 (2005) 2100–2110, doi:10.1101/gad.1346005.
[41] K. Yoshida, Y. Miki, Role of BRCA1 and BRCA2 as regulators of DNA repair, transcription, and cell cycle in response to DNA damage, Cancer Sci. 95 (2004) 866–871, doi:10.1111/j.1349-7006.2004.tb02195.x.
[42] T.A. Mochan, M. Venere, R.A.J. DiTullio, T.D. Halazonetis, 53BP1 and NFBD1/MDC1-Nbs1 function in parallel interacting pathways activating ataxia-telangiectasia mutated (ATM) in response to DNA damage, Cancer Res. 63 (2003) 8586–8591.
[43] P.-P. Wu, H.-W. Chung, K.-C. Liu, R.S.-C. Wu, J.-S. Yang, N.-Y. Tang, C. Lo, T.-C. Hsia, C.-C. Yu, F.-S. Chueh, S.-S. Lin, J.-G. Chung, Diallyl sulfide induces cell cycle arrest and apoptosis in HeLa human cervical cancer cells through the p53, caspase- and mitochondria-dependent pathways, Int. J. Oncol. 38 (2011) 1605–1613, doi:10.3892/ijo.2011.973.
[44] W. Luo, S. Li, B. Peng, Y. Ye, X. Deng, K. Yao, Embryonic stem cells markers SOX2, OCT4 and nanog expression and their correlations with epithelial-mesenchymal transition in nasopharyngeal carcinoma, PLoS. One 8 (2013) e56324, doi:10.1371/journal.pone.0056324.
[45] M.P. Stemmler, R.L. Eccles, S. Brabletz, T. Brabletz, Non-redundant functions of EMT transcription factors, Nat. Cell Biol. 21 (2019) 102–112, doi:10.1038/s41556-018-0196-y.
[46] N. Zhao, M.C. Woodle, A.J. Mixson, Advances in delivery systems for doxorubicin, J. Nanomed. Nanotechnol. 9 (2018) 519, doi:10.4172/2157-7439.1000519.
[47] A.F. Chambers, A.C. Groom, I.C. MacDonald, Dissemination and growth of cancer cells in metastatic sites, Nat. Rev. Cancer 2 (2002) 563–572, doi:10.1038/nrc865.
[48] P. Redondo, P. Lloret, M. Idoate, S. Inoges, Expression and serum levels of MMP-2 and MMP-9 during human melanoma progression, Clin. Exp. Dermatol. 30 (2005) 541–545, doi:10.1111/j.1365-2230.2005.01849.x.
[49] U.B. Hofmann, J.R. Westphal, E.T. Waas, A.J. Zendman, I.M. Cornelissen, D.J. Ruiter, G.N. van Muijen, Matrix metalloproteinases in human melanoma cell lines and xenografts: increased expression of activated matrix metalloproteinase-2 (MMP-2) correlates with melanoma progression, Br. J. Cancer 81 (1999) 774–782, doi:10.1038/sj.bjc.6690763.
[50] H. Birkedal-Hansen, W.G. Moore, M.K. Bodden, L.J. Windsor, B. Birkedal-Hansen, A. DeCarlo, J.A. Engler, Matrix metalloproteinases: a review, Crit. Rev. Oral Biol. Med. 4 (1993) 197–250, doi:10.1177/10454411930040020401.
[51] D.S. Hipps, R.M. Hembry, A.J. Docherty, J.J. Reynolds, G. Murphy, Purification and characterization of human 72-kDa gelatinase (type IV collagenase). Use of immunolocalisation to demonstrate the non-coordinate regulation of the 72-kDa and 95-kDa gelatinases by human fibroblasts, Biol. Chem. Hoppe Seyler. 372 (1991) 287–296, doi:10.1515/bchm3.1991.372.1.287.
[52] A.H. Baker, D.R. Edwards, G. Murphy, Metalloproteinase inhibitors: biological actions and therapeutic opportunities, J. Cell Sci. 115 (2002) 3719–3727, doi:10.1242/jcs.00063.
[53] S. Guo, C.-X. Deng, Effect of stromal cells in tumor microenvironment on metastasis initiation, Int. J. Biol. Sci. 14 (2018) 2083–2093, doi:10.7150/ijbs.25720.
[54] I. Müller, D. Kulms, A 3D organotypic melanoma spheroid skin model, J. Vis. Exp. 57500 (2018), doi:10.3791/57500.
[55] E. Kim, S. Choi, B. Kang, J. Kong, Y. Kim, W.H. Yoon, H.-R. Lee, S. Kim, H.-M. Kim, H. Lee, C. Yang, Y.J. Lee, M. Kang, T.-Y. Roh, S. Jung, S. Kim, J.H. Ku, K. Shin, Creation of bladder assembloids mimicking tissue regeneration and cancer, Nature 588 (2020) 664–669, doi:10.1038/s41586-020-3034-x.
[56] J. Ogishima, A. Taguchi, A. Kawata, K. Kawana, M. Yoshida, Y. Yoshimatsu, M. Sato, H. Nakamura, Y. Kawata, A. Nishijima, A. Fujimoto, K. Tomio, K. Adachi, T. Nagamatsu, K. Oda, T. Kiyono, Y. Osuga, T. Fujii, The oncogene KRAS promotes cancer cell dissemination by stabilizing spheroid formation via the MEK pathway, BMC Cancer 18 (2018) 1201, doi:10.1186/s12885-018-4922-4.
[57] M.C. Whelan, D.R. Senger, Collagen I initiates endothelial cell morphogenesis by inducing actin polymerization through suppression of cyclic AMP and protein kinase A, J. Biol. Chem. 278 (2003) 327–334, doi:10.1074/jbc.M207554200.
[58] A.C. Newman, M.N. Nakatsu, W. Chou, P.D. Gershon, C.C.W. Hughes, The requirement for fibroblasts in angiogenesis: fibroblast-derived matrix proteins are essential for endothelial cell lumen formation, Mol. Biol. Cell 22 (2011) 3791–3800, doi:10.1091/mbc.E11-05-0393.
[59] R.R. Rao, A.W. Peterson, J. Ceccarelli, A.J. Putnam, J.P. Stegemann, Matrix composition regulates three-dimensional network formation by endothelial cells and mesenchymal stem cells in collagen/fibrin materials, Angiogenesis. 15 (2012) 253–264, doi:10.1007/s10456-012-9257-1.
[60] W.-H. Huang, M.-C. Chang, K.-S. Tsai, M.-C. Hung, H.-L. Chen, S.-C. Hung, Mesenchymal stem cells promote growth and angiogenesis of tumors in mice, Oncogene 32 (2013) 4343–4354, doi:10.1038/onc.2012.458.
[61] P.A. Soucy, L.H. Romer, Endothelial cell adhesion, signaling, and morphogenesis in fibroblast-derived matrix, Matrix Biol. 28 (2009) 273–283, doi:10.1016/j.matbio.2009.04.005.
[62] T. Menge, M. Gerber, K. Wataha, W. Reid, S. Guha, C.S. Cox, P. Dash, M.S. Reitz, A.Y. Khakoo, S. Pati, Human mesenchymal stem cells inhibit endothelial proliferation and angiogenesis via cell–cell contact through modulation of the VE-cadherin/β-catenin signaling pathway, Stem Cells Dev. 22 (2012) 148–157, doi:10.1089/scd.2012.0165.
[63] N.K. Haass, K.A. Beaumont, D.S. Hill, A. Anfosso, P. Mrass, M.A. Munoz, I. Kinjyo, W. Weninger, Real-time cell cycle imaging during melanoma growth, in-

vasion, and drug response, Pigment. Cell Melanoma Res. 27 (2014) 764–776, doi:10.1111/pcmr.12274.
[64] R.M. Sutherland, Cell and environment interactions in tumor microregions: the multicell spheroid model, Science (1979) 240 (1988) 177 LP–184, doi:10.1126/science.2451290.
[65] L.-B. Weiswald, D. Bellet, V. Dangles-Marie, Spherical cancer models in tumor biology, Neoplasia 17 (2015) 1–15, doi:10.1016/j.neo.2014.12.004.
[66] H.R. Byers, J. Bhawan, Pathologic parameters in the diagnosis and prognosis of primary cutaneous melanoma, Hematol. Oncol. Clin. North Am. 12 (1998) 717–735, doi:10.1016/S0889-8588(05)70020-4.
[67] B.R. Smoller, Histologic criteria for diagnosing primary cutaneous malignant melanoma, Modern Pathol. 19 (2006) S34–S40, doi:10.1038/modpathol.3800508.
[68] A. Amann, M. Zwierzina, S. Koeck, G. Gamerith, E. Pechriggl, J.M. Huber, E. Lorenz, J.M. Kelm, W. Hilbe, H. Zwierzina, J. Kern, Development of a 3D angiogenesis model to study tumour – endothelial cell interactions and the effects of anti-angiogenic drugs, Sci. Rep. 7 (2017) 2963, doi:10.1038/s41598-017-03010-6.
[69] S. Pasco, L. Ramont, F.-X. Maquart, J.C. Monboisse, Control of melanoma progression by various matrikines from basement membrane macromolecules, Crit. Rev. Oncol. Hematol. 49 (2004) 221–223, doi:10.1016/j.critrevonc.2003.09.006.
[70] K.T. Tran, P. Lamb, J.-S. Deng, Matrikines and matricryptins: implications for cutaneous cancers and skin repair, J. Dermatol. Sci. 40 (2005) 11–20, doi:10.1016/j.jdermsci.2005.05.001.
[71] L. Batelja-Vuletic, C. Tomasovic-Loncaric, M. Ceppi, M. Bruzzone, A. Fucic, K. Krstanac, V. Boras Vucicevic, Comparison of androgen receptor, VEGF, HIF-1, Ki67 and MMP9 expression between non-metastatic and metastatic stages in stromal and tumor cells of oral squamous cell Carcinoma, Life 11 (2021), doi:10.3390/life11040336.
[72] E. Richardsen, R.D. Uglehus, S.H. Johnsen, L.-T. Busund, Immunohistochemical expression of epithelial and stromal immunomodulatory signalling molecules is a prognostic indicator in breast cancer, BMC. Res. Notes 5 (2012) 110, doi:10.1186/1756-0500-5-110.
[73] K.G. Mitchell, E.R. Parra, D.B. Nelson, J. Zhang, I.I. Wistuba, J. Fujimoto, J.A. Roth, M.B. Antonoff, E.M. Corsini, A.A. Vaporciyan, W.L. Hofstetter, R.J. Mehran, S.G. Swisher, D.C. Rice, B. Sepesi, G.L. Walsh, C. Behrens, N. Kalhor, A. Weissferdt, C.A. Moran, J.J. Lee, Tumor cellular proliferation is associated with enhanced immune checkpoint expression in stage I non–small cell lung cancer, J. Thorac. Cardiovasc. Surg. 158 (2019) 911-919.e6, doi:10.1016/j.jtcvs.2019.04.084.
[74] J.E. Visvader, G.J. Lindeman, Cancer stem cells: current status and evolving complexities, Cell Stem Cell 10 (2012) 717–728, doi:10.1016/j.stem.2012.05.007.
[75] L. Yang, P. Shi, G. Zhao, J. Xu, W. Peng, J. Zhang, G. Zhang, X. Wang, Z. Dong, F. Chen, H. Cui, Targeting cancer stem cell pathways for cancer therapy, Signal. Transduct. Target. Ther. 5 (2020) 8, doi:10.1038/s41392-020-0110-5.
[76] M. Al Mamun, K. Mannoor, J. Cao, F. Qadri, X. Song, SOX2 in cancer stemness: tumor malignancy and therapeutic potentials, J. Mol. Cell Biol. 12 (2020) 85–98, doi:10.1093/jmcb/mjy080.
[77] X. Wang, J. Dai, Concise review: isoforms of OCT4 contribute to the confusing diversity in stem cell biology, Stem Cells 28 (2010) 885–893, doi:10.1002/stem.419.
[78] C.T.X. Silva, V.A. Saddi, K.S.F. e Silva, D.M. Sugita, L.A. Guillo, Expression of the cancer stem cell marker OCT4 is associated with worse prognosis and survival in cutaneous melanoma, Melanoma Res. 31 (2021).
[79] F. Paino, M. La Noce, D. Di Nucci, Human adipose stem cell differentiation is highly affected by cancer cells both *in vitro* and *in vivo*: implication for autologous fat grafting, Cell Death Dis 8 (2018) e2568, doi:10.1038/cddis.2016.308.
[80] C. Melzer, J. von der Ohe, H. Lehnert, H. Ungefroren, R. Hass, Cancer stem cell niche models and contribution by mesenchymal stroma/stem cells, Mol. Cancer 16 (2017) 28, doi:10.1186/s12943-017-0595-x.
[81] M. Ohanna, C. Bonet, K. Bille, M. Allegra, I. Davidson, P. Bahadoran, J.-P. Lacour, R. Ballotti, C. Bertolotto, SIRT1 promotes proliferation and inhibits the senescence-like phenotype in human melanoma cells, Oncotarget. 5 (2014) 2085.
[82] M.J. Wilking, C. Singh, M. Nihal, W. Zhong, N. Ahmad, SIRT1 deacetylase is overexpressed in human melanoma and its small molecule inhibition imparts anti-proliferative response via p53 activation, Arch. Biochem. Biophys. 563 (2014) 94–100, doi:10.1016/j.abb.2014.04.001.
[83] E. Khodadadi, S.M. Mir, M.Y. Memar, H. Sadeghi, M. Kashiri, M. Faeghiniya, Z. Jamalpoor, M. Sheikh Arabi, Shelterin complex at telomeres: roles in cancers, Gene Rep. 23 (2021) 101174, doi:10.1016/j.genrep.2021.101174.
[84] J. Cherfils-Vicini, E. Gilson, Inhibiting TRF1 upstream signaling pathways to target telomeres in cancer cells, EMBo Mol. Med. 11 (2019) e10845, doi:10.15252/emmm.201910845.
[85] Z.-Z. Zhang, Y.J.C. Liu, X.-L. Yin, P. Zhan, Y. Gu, X.-Z. Ni, Loss of BRCA1 expression leads to worse survival in patients with gastric carcinoma, World J. Gastroenterol. 19 (2013) 1968–1974, doi:10.3748/wjg.v19.i12.1968.
[86] M.E. Thompson, R.A. Jensen, P.S. Obermiller, D.L. Page, J.T. Holt, Decreased expression of BRCA1 accelerates growth and is often present during sporadic breast cancer progression, Nat. Genet. 9 (1995) 444–450, doi:10.1038/ng0495-444.
[87] G. De Gregoriis, J.A. Ramos, P.V. Fernandes, G.M. Vignal, R.C. Brianese, D.M. Carraro, A.N. Monteiro, C.J. Struchiner, G. Suarez-Kurtz, R. Vianna-Jorge, M.A. de Carvalho, DNA repair genes PAXIP1 and TP53BP1 expression is associated with breast cancer prognosis, Cancer Biol. Ther. 18 (2017) 439–449, doi:10.1080/15384047.2017.1323590.
[88] N.L. Ausborn, T. Wang, S.C. Wentz, M.K. Washington, N.B. Merchant, Z. Zhao, Y. Shyr, A.B. Chakravarthy, F. Xia, 53BP1 expression is a modifier of the prognostic value of lymph node ratio and CA 19–9 in pancreatic adenocarcinoma, BMC Cancer 13 (2013) 155, doi:10.1186/1471-2407-13-155.
[89] M. Croke, M.A. Neumann, D.A. Grotsky, R. Kreienkamp, S.C. Yaddanapudi, S. Gonzalo, Differences in 53BP1 and BRCA1 regulation between cycling and non-cycling cells, Cell Cycle 12 (2013) 3629–3639, doi:10.4161/cc.26582.
[90] C. Escribano-Díaz, A. Orthwein, A. Fradet-Turcotte, M. Xing, J.T.F. Young, J. Tkáč, M.A. Cook, A.P. Rosebrock, M. Munro, M.D. Canny, D. Xu, D. Durocher, A cell cycle-dependent regulatory circuit composed of 53BP1-RIF1 and BRCA1-CtIP controls DNA repair pathway choice, Mol. Cell 49 (2013) 872–883, doi:10.1016/j.molcel.2013.01.001.
[91] S.F. Bunting, E. Callén, N. Wong, H.-T. Chen, F. Polato, A. Gunn, A. Bothmer, N. Feldhahn, O. Fernandez-Capetillo, L. Cao, X. Xu, C.-X. Deng, T. Finkel, M. Nussenzweig, J.M. Stark, A. Nussenzweig, 53BP1 inhibits homologous recombination in Brca1-deficient cells by blocking resection of DNA breaks, Cell 141 (2010) 243–254, doi:10.1016/j.cell.2010.03.012.
[92] E. Imyanitov, A. Sokolenko, T. Gorodnova, E. Savonevich, A. Ivantsov, E. Preobrazhenskaya, A. Togo, I. Berlev, Primary ovarian carcinomas arising in BRCA1 mutation carriers contain a small fraction of BRCA1-proficient cells, which rapidly repopulate tumor mass during neoadjuvant chemotherapy but become outgrown by BRCA1-deficient clones during platinum-free intervals, Ann. Oncol. 30 (2019) v763, doi:10.1093/annonc/mdz268.006.
[93] H. Fettke, C. Dai, E.M. Kwan, T. Zheng, P. Du, N. Ng, P. Bukczynska, M. Docanto, L. Kostos, S. Foroughi, S. Brown, L.-J.K. Graham, K. Mahon, L.G. Horvath, S. Jia, M. Kohli, A.A. Azad, BRCA-deficient metastatic prostate cancer has an adverse prognosis and distinct genomic phenotype, EBioMedicine (2023) 95, doi:10.1016/j.ebiom.2023.104738.
[94] J. Puppe, R. Drost, X. Liu, S.A. Joosse, B. Evers, P. Cornelissen-Steijger, P. Nederlof, Q. Yu, J. Jonkers, M. van Lohuizen, A.M. Pietersen, BRCA1-deficient mammary tumor cells are dependent on EZH2 expression and sensitive to Polycomb Repressive Complex 2-inhibitor 3-deazaneplanocin A, Breast Cancer Res. 11 (2009) R63, doi:10.1186/bcr2354.
[95] J. Gros, C.J. Tabin, Vertebrate limb bud formation is initiated by localized epithelial-to-mesenchymal transition, Science 343 (2014) 1253–1256, doi:10.1126/science.1248228.
[96] Y. Huang, W. Hong, X. Wei, The molecular mechanisms and therapeutic strategies of EMT in tumor progression and metastasis, J. Hematol. Oncol. 15 (2022) 129, doi:10.1186/s13045-022-01347-8.
[97] M. Correa-Costa, V. Andrade-Oliveira, T.T. Braga, A. Castoldi, C.F. Aguiar, C.S.T. Origassa, A.C.D. Rodas, M.I. Hiyane, D.M.A.C. Malheiros, F.J.O. Rios, S. Jancar, N.O.S. Câmara, Activation of platelet-activating factor receptor exacerbates renal inflammation and promotes fibrosis, Lab. Investig. 94 (2014) 455–466, doi:10.1038/labinvest.2013.155.
[98] T. Brabletz, R. Kalluri, M.A. Nieto, R.A. Weinberg, EMT in cancer, Nat. Rev. Cancer 18 (2018) 128–134, doi:10.1038/nrc.2017.118.
[99] R. Kalluri, E.G. Neilson, Epithelial-mesenchymal transition and its implications for fibrosis, J. Clin. Invest. 112 (2003) 1776–1784.
[100] M.K. Wendt, M.A. Taylor, B.J. Schiemann, W.P. Schiemann, Down-regulation of epithelial cadherin is required to initiate metastatic outgrowth of breast cancer, Mol. Biol. Cell 22 (2011) 2423–2435, doi:10.1091/mbc.E11-04-0306.
[101] C.E. Aban, A. Lombardi, G. Neiman, M.C. Biani, A. La Greca, A. Waisman, L.N. Moro, G. Sevlever, S. Miriuka, C. Luzzani, Downregulation of E-cadherin in pluripotent stem cells triggers partial EMT, Sci. Rep. 11 (2021) 2048, doi:10.1038/s41598-021-81735-1.
[102] E. Burandt, F. Lübbersmeyer, N. Gorbokon, F. Büscheck, A.M. Luebke, A. Menz, M. Kluth, C. Hube-Magg, A. Hinsch, D. Höflmayer, S. Weidemann, C. Fraune, K. Möller, F. Jacobsen, P. Lebok, T.S. Clauditz, G. Sauter, R. Simon, R. Uhlig, W. Wilczak, S. Steurer, S. Minner, R. Krech, D. Dum, T. Krech, A.H. Marx, C. Bernreuther, E-Cadherin expression in human tumors: a tissue microarray study on 10,851 tumors, Biomark. Res. 9 (2021) 44, doi:10.1186/s40364-021-00299-4.
[103] Y. Luo, T. Yu, Q. Zhang, Q. Fu, Y. Hu, M. Xiang, H. Peng, T. Zheng, L. Lu, H. Shi, Upregulated N-cadherin expression is associated with poor prognosis in epithelial-derived solid tumours: a meta-analysis, Eur. J. Clin. Invest. 48 (2018), doi:10.1111/eci.12903.
[104] K.M. Mrozik, O.W. Blaschuk, C.M. Cheong, A.C.W. Zannettino, K. Vandyke, N-cadherin in cancer metastasis, its emerging role in haematological malignancies and potential as a therapeutic target in cancer, BMC Cancer 18 (2018) 939, doi:10.1186/s12885-018-4845-0.
[105] Z.-Q. Cao, Z. Wang, P. Leng, Aberrant N-cadherin expression in cancer, Biomed. Pharmacother. 118 (2019) 109320, doi:10.1016/j.biopha.2019.109320.
[106] J. Caramel, E. Papadogeorgakis, L. Hill, G.J. Browne, G. Richard, A. Wierinckx, G. Saldanha, J. Osborne, P. Hutchinson, G. Tse, J. Lachuer, A. Puisieux, J.H. Pringle, S. Ansieau, E. Tulchinsky, A switch in the expression of embryonic EMT-inducers drives the development of malignant melanoma, Cancer Cell 24 (2013) 466–480, doi:10.1016/j.ccr.2013.08.018.
[107] M. Li, B. Zhang, B. Sun, X. Wang, X. Ban, T. Sun, Z. Liu, X. Zhao, A novel function for vimentin: the potential biomarker for predicting melanoma hematogenous metastasis, J. Exp. Clinic. Cancer Res. 29 (2010) 109, doi:10.1186/1756-9966-29-109.
[108] S.R. Alonso, L. Tracey, P. Ortiz, B. Pérez-Gómez, J. Palacios, M. Pollán, J. Linares, S. Serrano, A.I. Sáez-Castillo, L. Sánchez, R. Pajares, A. Sánchez-Aguilera,

M.J. Artiga, M.A. Piris, J.L. Rodríguez-Peralto, A high-throughput study in melanoma identifies epithelial-mesenchymal transition as a major determinant of metastasis, Cancer Res. 67 (2007) 3450–3460, doi:10.1158/0008-5472.CAN-06-3481.
[109] A. Dongre, R.A. Weinberg, New insights into the mechanisms of epithelial–mesenchymal transition and implications for cancer, Nat. Rev. Mol. Cell Biol. 20 (2019) 69–84, doi:10.1038/s41580-018-0080-4.
[110] X. Ye, W.L. Tam, T. Shibue, Y. Kaygusuz, F. Reinhardt, E. Ng Eaton, R.A. Weinberg, Distinct EMT programs control normal mammary stem cells and tumour-initiating cells, Nature 525 (2015) 256–260, doi:10.1038/nature14897.
[111] E. Licarete, V.F. Rauca, L. Luput, D. Drotar, I. Stejerean, L. Patras, B. Dume, V.A. Toma, A. Porfire, C. Gherman, A. Sesarman, M. Banciu, Overcoming intrinsic doxorubicin resistance in melanoma by anti-angiogenic and anti-metastatic effects of liposomal prednisolone phosphate on tumor microenvironment, Int. J. Mol. Sci. 21 (2020) 2968, doi:10.3390/ijms21082968.
[112] K. Harati, A. Daigeler, T. Hirsch, F. Jacobsen, B. Behr, C. Wallner, M. Lehnhardt, M. Becerikli, Tumor-associated fibroblasts promote the proliferation and decrease the doxorubicin sensitivity of liposarcoma cells, Int. J. Mol. Med. 37 (2016) 1535–1541, doi:10.3892/ijmm.2016.2556.
[113] E.J. Ruiz, F. Oeztuerk-Winder, J.-J. Ventura, A paracrine network regulates the cross-talk between human lung stem cells and the stroma, Nat. Commun. 5 (2014) 3175, doi:10.1038/ncomms4175.
[114] M. Humayun, J.M. Ayuso, R.A. Brenneke, M. Virumbrales-Muñoz, K. Lugo-Cintrón, S. Kerr, S.M. Ponik, D.J. Beebe, Elucidating cancer-vascular paracrine signaling using a human organotypic breast cancer cell extravasation model, Biomaterials 270 (2021) 120640, doi:10.1016/j.biomaterials.2020.120640.
[115] K. Räsänen, M. Herlyn, Paracrine signaling between carcinoma cells and mesenchymal stem cells generates cancer stem cell niche via epithelial–mesenchymal transition, Cancer Discov. 2 (2012) 775 LP–777, doi:10.1158/2159-8290.CD-12-0312.
[116] W. Bode, K. Maskos, Structural basis of the matrix metalloproteinases and their physiological inhibitors, the tissue inhibitors of metalloproteinases, Biol. Chem. 384 (2003) 863–872, doi:10.1515/BC.2003.097.
[117] H. Laronha, J. Caldeira, Structure and function of human matrix metalloproteinases, Cells 9 (2020) 1076, doi:10.3390/cells9051076.
[118] R. Fukushima, A. Kasamatsu, D. Nakashima, M. Higo, K. Fushimi, H. Kasama, Y. Endo-Sakamoto, M. Shiiba, H. Tanzawa, K. Uzawa, Overexpression of translocation associated membrane protein 2 leading to cancer-associated matrix metalloproteinase activation as a putative metastatic factor for human oral cancer, J. Cancer 9 (2018) 3326–3333, doi:10.7150/jca.25666.
[119] M. Miyake, S. Goodison, A. Lawton, E. Gomes-Giacoia, C.J. Rosser, Angiogenin promotes tumoral growth and angiogenesis by regulating matrix metallopeptidase-2 expression via the ERK1/2 pathway, Oncogene 34 (2015) 890–901, doi:10.1038/onc.2014.2.
[120] T. Saito, A. Kasamatsu, K. Ogawara, I. Miyamoto, K. Saito, M. Iyoda, T. Suzuki, Y. Endo-Sakamoto, M. Shiiba, H. Tanzawa, K. Uzawa, Semaphorin7A promotion of tumoral growth and metastasis in human oral cancer by regulation of G1 cell cycle and matrix metalloproteases: possible contribution to tumoral angiogenesis, PLoS ONE 10 (2015) e0137923.
[121] A.M. Montgomery, B.M. Mueller, R.A. Reisfeld, S.M. Taylor, Y.A. DeClerck, Effect of tissue inhibitor of the matrix metalloproteinases-2 expression on the growth and spontaneous metastasis of a human melanoma cell line, Cancer Res. 54 (1994) 5467–5473.
[122] D.R. Bielenberg, B.R. Zetter, The contribution of angiogenesis to the process of metastasis, Cancer J 21 (2015).
[123] H. Nagase, R. Visse, G. Murphy, Structure and function of matrix metalloproteinases and TIMPs, Cardiovasc. Res. 69 (2006) 562–573, doi:10.1016/j.cardiores.2005.12.002.
[124] J.J. van den Oord, L. Paemen, G. Opdenakker, C. de Wolf-Peeters, Expression of gelatinase B and the extracellular matrix metalloproteinase inducer EMMPRIN in benign and malignant pigment cell lesions of the skin, Am. J. Pathol. 151 (1997) 665–670.
[125] U.B. Hofmann, A.A.O. Eggert, K. Blass, E.-B. Bröcker, J.C. Becker, Expression of matrix metalloproteinases in the microenvironment of spontaneous and experimental melanoma metastases reflects the requirements for tumor formation, Cancer Res. 63 (2003) 8221 LP –8225.
[126] M. Polette, C. Clavel, M. Cockett, S. Girod de Bentzmann, G. Murphy, P. Birembaut, Detection and localization of mRNAs encoding matrix metalloproteinases and their tissue inhibitor in human breast pathology, Invas. Metast. 13 (1993) 31–37.
[127] L. Ziani, T. Ben Safta-Saadoun, J. Gourbeix, A. Cavalcanti, C. Robert, G. Favre, S. Chouaib, J. Thiery, Melanoma-associated fibroblasts decrease tumor cell susceptibility to NK cell-mediated killing through matrix-metalloproteinases secretion, Oncotarget 8 (2017) 19780–19794, doi:10.18632/oncotarget.15540.
[128] C.B. Mitchell, G.M. O'Neill, Cooperative cell invasion: matrix metalloproteinase–mediated incorporation between cells, Mol. Biol. Cell 27 (2016) 3284–3292, doi:10.1091/mbc.E16-03-0194.
[129] A. Chapman, L. Fernandez del Ama, J. Ferguson, J. Kamarashev, C. Wellbrock, A. Hurlstone, Heterogeneous tumor subpopulations cooperate to drive invasion, Cell Rep. 8 (2014) 688–695, doi:10.1016/j.celrep.2014.06.045.
[130] E.J. Rowling, Z. Miskolczi, R. Nagaraju, D.J. Wilcock, P. Wang, B. Telfer, Y. Li, I. Lasheras-Otero, M. Redondo-Muñoz, A.D. Sharrocks, I. Arozarena, C. Wellbrock, Cooperative behaviour and phenotype plasticity evolve during melanoma progression, Pigment. Cell Melanoma Res. 33 (2020) 695–708, doi:10.1111/pcmr.12873.
[131] Y. Hegerfeldt, M. Tusch, E.B. Bröcker, P. Friedl, Collective cell movement in primary melanoma explants: plasticity of cell-cell interaction, beta1-integrin function, and migration strategies, Cancer Res. 62 (7) (2002) 2125–2130 https://api.semanticscholar.org/CorpusID:12787636.
[132] W.G. Stetler-Stevenson, Tissue inhibitors of metalloproteinases in cell signaling: metalloproteinase-independent biological activities, Sci. Signal. 1 (2008) re6–re6, doi:10.1126/scisignal.127re6.
[133] D. Bourboulia, W.G. Stetler-Stevenson, Matrix metalloproteinases (MMPs) and tissue inhibitors of metalloproteinases (TIMPs): positive and negative regulators in tumor cell adhesion, Semin. Cancer Biol. 20 (2010) 161–168, doi:10.1016/j.semcancer.2010.05.002.
[134] X. Wen, J.-Q. Wu, W. Peng, J.-F. Feng, J.-H. Tang, MicroRNA-377 predicts poor clinical outcome of gastric cancer and induces tumorigenesis by targeting multiple tumor-suppressor genes, Oncol. Rep. 34 (2015) 203–210, doi:10.3892/or.2015.3981.
[135] A. Rotte, M. Martinka, G. Li, MMP2 expression is a prognostic marker for primary melanoma patients, Cell Oncol. 35 (2012) 207–216, doi:10.1007/s13402-012-0080-x.
[136] L. Perrin, B. Bayarmagnai, E. Tüzel, B. Gligorijevic, Invadopodia enable cooperative invasion and metastasis of breast cancer cells, bioRxiv (2021) 2021.02.13.431047, doi:10.1101/2021.02.13.431047.